Geochemistry, Geophysics, Geosystems®

RESEARCH ARTICLE
10.1029/2024GC011728

The Jurassic–Cretaceous Transition in the Slovenian Basin (Alpine Atlantic): Further Evidence for Palaeoenvironmental Record in Pelagic Sediments

D. G. Lodowski[1], J. Grabowski[1], B. Rožič[2], P. Žvab-Rožič[2], D. Reháková[3], L. Slapnik[2], J. Iwańczuk[1], A. Chmielewski[1], and A. Teodorski[4]

[1]Polish Geological Institute–National Research Institute, Warsaw, Poland, [2]Department of Geology, Faculty of Natural Sciences and Engineering, University of Ljubljana, Ljubljana, Slovenia, [3]Department of Geology and Paleontology, Comenius University in Bratislava, Bratislava, Slovakia, [4]Faculty of Geology, University of Warsaw, Warsaw, Poland

Abstract Over the vast area of present-day Europe, the Tithonian–Berriasian transition was a time of climate aridization, which was supposedly related to the more general trend of the latest Jurassic–earliest Cretaceous cooling and restrictions in atmospheric circulation. Recent studies suggest that such conditions affected also some other paleoenvironmental processes such as monsoonal upwellings, seafloor ventilation and circulation of nutrients within the water column. In order to test this model, the uppermost Jurassic–lowermost Cretaceous sedimentary succession of the Slovenian Basin was correlated with a reference data from the Bakony Basin (Transdanubian Range, Hungary). Stratigraphic calibration was ensured by integrated stratigraphy, utilizing bio- (calpionellids, calcareous dinocysts) and chemostratigraphic tools ($\delta^{13}C$ stratigraphy) as well as regional correlations of magnetic susceptibility and terrigenous input. Paleoclimate, paleoredox and paleoproductivity conditions were evaluated based on various geochemical proxies. Both the Slovenian and the Bakony basin sections were found to document late Tithonian–early Berriasian climate aridization as well as related signals of seafloor hypoxia and elevated accumulations of micronutrients. Significant geochemical contrast between the basal (lower Tithonian) radiolarites and overlying upper Tithonian–Berriasian carbonates evidences the inverse relation between the surface productivity and the amount of nutrient-type trace metals buried in sediments. The rhythm of paleoclimatically controlled environmental changes, with relatively humid early Tithonian, arid late Tithonian–early Berriasian, and again humid late Berriasian, correlates with those estimated for Vocontian Basin (SE France) and the Sub-Boreal domain of Western and Central Europe. This indicates that climatic stratigraphy is a useful tool for global correlation of the Jurassic/Cretaceous boundary interval.

Plain Language Summary During the Mesozoic, much of the present-day Alpine orogenic belt (Alps–Carpathians–Dinarides) constituted the westernmost part of the so-called Neotethys Ocean. Recent studies suggest that the gradual cooling during the Jurassic/Cretaceous transition affected this area by weakening of monsoons, what caused significant aridization. In addition, changes in atmospheric circulation are thought to have had an impact also on oceanographic conditions and the intensity of (wind-induced) upwelling currents among others. In this study, we attempt to test the above model by comparing the geochemical signals obtained from sedimentary successions of western Slovenia (Slovenian Basin) and western Hungary (Transdanubian Range). Our study confirms the hypothesis that late Tithonian–early Berriasian (ca. 145–140 Ma) climate aridization was associated with less intense mixing of the water column. This, in turn, limited the availability of oxygen at the seafloor on one hand, and increased the burial of nutrients on the other. Accordingly, the results of this study not only provide new data on the latest Jurassic–earliest Cretaceous sedimentary trends and events but also contribute to our understanding of a complex relationships between the state of atmosphere (climate) and its impact on marine environments and support the global definition of the Jurassic/Cretaceous boundary.

Key Points:

- Geochemical contrast between radiolarites and limestones evidences the inverse relation between surface productivity and nutrient burial
- Arid climate of the Tithonian–Berriasian transition was associated with seafloor hypoxia and elevated accumulations of micronutrients
- A minor, but well pronounced peak in $\delta^{13}C$ is characteristic for the lower/upper Berriasian boundary interval

Correspondence to:
D. G. Lodowski,
damian.lodowski@pgi.gov.pl

Citation:
Lodowski, D. G., Grabowski, J., Rožič, B., Žvab-Rožič, P., Reháková, D., Slapnik, L., et al. (2024). The Jurassic–Cretaceous transition in the Slovenian Basin (Alpine Atlantic): Further evidence for palaeoenvironmental record in pelagic sediments. *Geochemistry, Geophysics, Geosystems*, *25*, e2024GC011728. https://doi.org/10.1029/2024GC011728

Received 27 JUN 2024
Accepted 7 NOV 2024

Author Contributions:
Conceptualization: D. G. Lodowski, J. Grabowski
Investigation: D. G. Lodowski, J. Grabowski, B. Rožič, P. Žvab-Rožič, D. Reháková, L. Slapnik, J. Iwańczuk, A. Chmielewski, A. Teodorski
Methodology: D. G. Lodowski
Supervision: J. Grabowski
Validation: D. G. Lodowski, J. Grabowski, B. Rožič
Writing – original draft: D. G. Lodowski, J. Grabowski, B. Rožič
Writing – review & editing: D. G. Lodowski

1. Introduction

The latest Jurassic and Early Cretaceous likely represents the coolest interval in the Mesozoic Era (TEBCI: Tithonian–early Barremian Cool Interval), approaching even an icehouse state (Scotese et al., 2021) with possible developments of ice sheets on shelf margins at high latitudes (e.g., Alley et al., 2020; Cavalheiro et al., 2021; Price, 1999; van der Meer et al., 2022) and glendonites in the fossil record (e.g., Rogov et al., 2017, 2021 and

references therein). Global stratigraphic correlation in the late Tithonian and early Berriasian (Jurassic/Cretaceous boundary interval) is hampered by biotic provincialism (e.g., Cope, 2008; Wimbledon et al., 2020) and sea-level regression (e.g., Hallam, 2001; Haq, 2014, 2018; van der Meer et al., 2022). In this context, integration of biotic and palaeoenvironmental trends can help overcome difficulties which hitherto prevented a consensus on the global definition of the J/K boundary (Grabowski et al., 2022).

Numerous papers raised the importance of arid/humid climatic cycles in the J/K boundary interval (e.g., Abbink et al., 2001; Föllmi, 2012; Grabowski, Chmielewski, et al., 2021; Hallam et al., 1991; Morales et al., 2013; Riboulleau et al., 2003; Schneider et al., 2018; Schnyder et al., 2006). In their recent paper, Lodowski, Szives, et al. (2024) provided a comprehensive paleoenvironmental model in which the latest Jurassic–earliest Cretaceous sedimentary processes recognized in the Bakony Basin sections (Transdanubian Range, Hungary) were associated with late Tithonian–early Berriasian cooling and aridization. This model utilizes the fact that continents are much more prone to (over)heating than the oceans. Therefore, in a warm and free of large ice caps Earth scenario, climate cooling reduces the thermal gradient occurring between land and ocean (see e.g., Trujillo & Thurman, 2011). This, in turn, weakens large-scale atmospheric circulation, decreasing the intensity of monsoons among other climatic phenomena and driving aridization. Lodowski, Szives, et al. (2024) considered that lowered atmospheric energy during the Tithonian/Berriasian transition restricted oceanographic processes, such as monsoonal (wind-induced) upwelling (see also De Wever et al., 2014). This would weaken mixing of the water column, resulting in the seafloor hypoxia and promoting burial of micronutrients due to disturbed nutrient shuttle mechanism.

Even though the model of Lodowski, Szives, et al. (2024) provides a consistent explanation of the data documented in the Transdanubian Range successions, it assumes the occurrence of large-scale processes that would have affected other sedimentary zones of the Alpine Atlantic ocean. This study attempts to test the model of Lodowski, Szives, et al. (2024) utilizing data collected in the uppermost Jurassic–lowermost Cretaceous succession of the neighboring Slovenian Basin (Petrovo Brdo section, NE Slovenia; Figure 1). A comparison between paleogeographically close basins allows testing whether they document common processes while limiting risks associated with large distance correlations, when regional, supraregional and/or global signals can be overprinted by various local processes. As a result, various paleoclimate, seafloor oxidation and paleoproductivity proxies from the Slovenian Basin and the Transdanubian Range are compared and interpreted in terms of their significance for the latest Jurassic–earliest Cretaceous paleoclimate and oceanographic conditions in the area of the Alpine Atlantic ocean.

2. Geological Setting

2.1. Geological Background

The Slovenian Basin preserves the largest and most continuous Mesozoic deep-marine sedimentary succession of the eastern part of the Adria microplate (Rožič, 2016). It was an approximately E–W extending basin that originated in the Middle Triassic during the opening of the Neotethys Ocean. It deepened progressively during Jurassic due to the opening of the Alpine Tethys Ocean, and lasted until the latest Cretaceous, when it turned into a foreland basin of the Alpine-Dinaric orogen (Buser, 1989, 1996; Rožič, 2009; Vrabec et al., 2009). Since the end of the Early Jurassic the basin became dominated by pelagic deposition, that is: (a) Toarcian marls of the Perbla Formation; (b) Aalenian–lower Tithonian siliceous limestones and radiolarian cherts of Tolmin Formation; and (c) the upper Tithonian–Berriasian calpionellid limestones of the Biancone Limestone Formation (Goričan, Pavšič, & Rožič, 2012; Goričan, Kosir, & Rožič, 2012; Rožič, 2009; Rožič & Šmuc, 2011). The Lower Cretaceous (Valanginian–mid Aptian) is missing, so that the succession is unconformably overlained by the uppermost Aptian–Turonian Lower Flyschoid Formation (Goričan, Pavšič, & Rožič, 2012; Goričan, Kosir, & Rožič, 2012; Rožič, 2005). The upcoming collision between the Adriatic Plate and the Tisza Megaunit resulted in the deposition of Coniacian–Campanian carbonate turbidites of the Volče Formation. Finally, the Slovenian Basin was filled by carbonate breccias and mixed siliciclastic-carbonate flysh-type deposits by the end of the Cretaceous (Goričan, Pavšič, & Rožič, 2012; Goričan, Kosir, & Rožič, 2012; Vrabec et al., 2009).

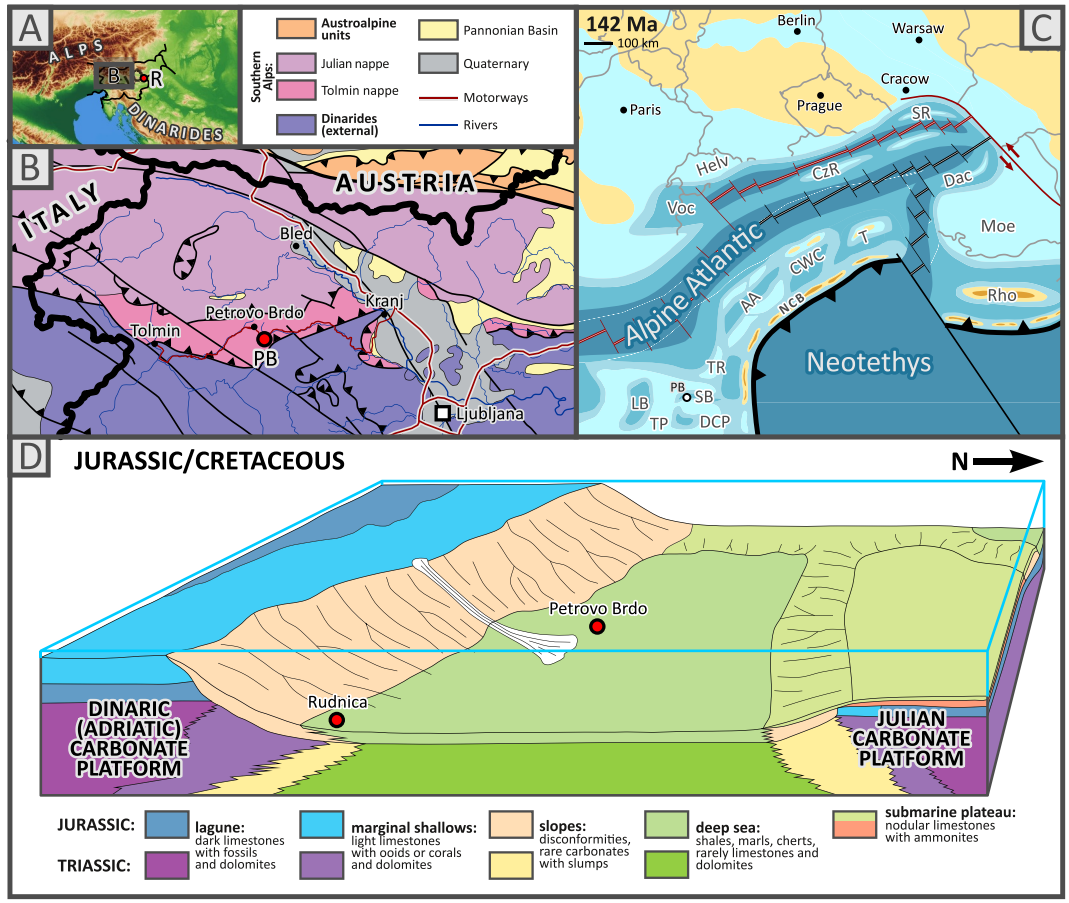

Figure 1. Geological framework of the Petrovo Brdo section. (a) localization in the context of Alps and Dinarides; (b) tectonic context of the northwestern Slovenia (modified after Placer, 2008); (c) paleogeographic map of the Alpine Atlantic and western Neotethys (modified after Lodowski et al., 2024); (d) schematic paleobathymetric reconstruction of the Slovenian Basin. Abbreviations: AA—Austroalpine; CWC—Central West Carpathians; CzR—Czorsztyn Ridge; Dac—Dacia; DCP—Dincaric Carbonate Platform; Helv—Helvetic shelf; LB—Lombardian Basin; Moe—Moesian Platform; NCB—Neotethyan Collision Belt; PB—Petrovo Brdo section; R—Rudnica section; Rho—Rhodopes; SB—Slovenian Basin; SR—Silesian Ridge; T—Tisia; TP—Trento Plateau; TR—Transdanubian Range; Voc—Vocontian Basin.

2.2. Section Descriptions

2.2.1. Petrovo Brdo

Petrovo Brdo is located in the foothills of the Julian Alps (western Slovenia) in the upper part of the Selška Sora river valley, close to its tributary, the Zadnja Sora stream (Figure 1). The section is exposed along the road 403 (46°11′38″N; 14°01′50″E), which runs from Železniki and Zali Log to Petrovo Brdo mountain pass.

Petrovo Brdo section covers the 40.7 m interval of the uppermost Jurassic–lowermost Cretaceous sediments (Figure 2). Basal 5 m are composed of thin-bedded (2–10 cm) greenish and often laminated radiolarian cherts intercalated by green shales (Tolmin Formation). Discontinuous dissolution seams are oriented parallel to the bedding and impregnated by Fe-hydroxides. Carbonates are dispersed within cherts and sometimes form patches of coarser (up to 200 μm) subhedral crystals. Green shale is interstratified, mostly in the form of thin bedding-plane films, but some thin layers (up to 2 cm) also occur. The thickest marly layer, which seals the Tolmin Fm., reaches 10 cm (5–5.1 m).

The following succession is composed of mostly light-colored pelagic limestone of the Biancone Limestone Fm. (BL Fm.; 5.1–40.7 m; Figure 2). Although it is generally monotonous in composition, some differences can be noted. The lower 8 m of the BL Fm. (up to meter 13) are made of light gray to almost white, thin- to medium-bedded (2–40 cm) pelagic limestones. The subsequent 9 m (up to meter 24) are generally thin-bedded, whereas

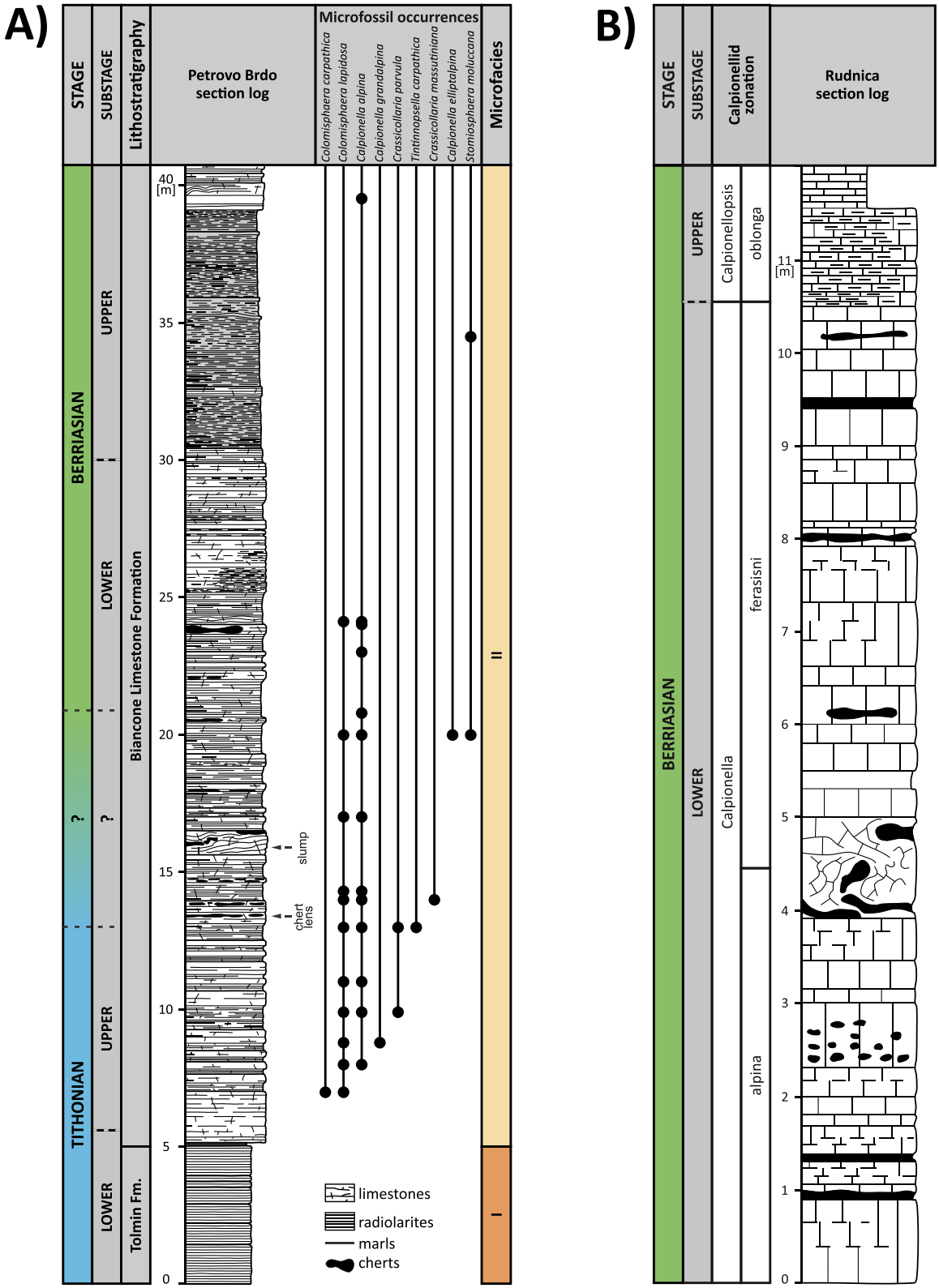

Figure 2. Microfossil occurences and microfacies of the Petrovo Brdo section (a) and the geological log of the Rudnica section (b; after Reháková & Rožič, 2019). Microfacies: I—silicified biomicrite with sponge spicules and radiolarians; II—wackestones with rare fossils.

thicker beds are additionally marked by chert nodules. Within this interval, at meter 16 of the section, a 90 cm thick syn-sedimentary slump was observed. Above meter 24, the rock turns more gray and marly, while bedding becomes less distinct and thinner, only sometimes forming thicker couplets. Between meters 30.4 and 39.1 limestones are thin-bedded and laminated; however, in most cases, bedding is indistinct and laterally discontinuous. The topmost 1.6 m of the section (39.1–40.7 m) depicts more distinct bedding again, reaching up to 30 cm in thickness. Although covered by vegetation, the overlying beds are most likely dominated by marls and/or shales, as evidenced by rubble within soil. On this basis, the top of the Petrovo Brdo section (meter 40.7) most likely constitutes the top of the Biancone Limestone Formation, and the base of the Lower Flyschoid Fm., as typical for this part of the basin (Demšar, 2016).

2.2.2. Rudnica

The Mount Rudnica section serves as a local reference section for stratigraphic calibration of the Petrovo Brdo section. It is located in the Sava Folds (eastern Slovenia), providing a record of the distal, drowned part of the Dinaric (Adriatic) Carbonate Platform on the southern rim of the Slovenian Basin (Figure 1d). The section was studied in detail by Reháková and Rožič (2019); therefore, here only the new magnetic susceptibility log is provided. The section consists of ca. 12 m thick lower and the lowermost upper Berriasian, developed in the Biancone Limestone (Figure 2).

3. Sampling and Methods

A total number of 97 stratigraphic horizons were sampled in the Petrovo Brdo section. The average sampling interval was 0.5 m; however, the resolution was increased within intervals of lithological changes. Samples were collected either by hand (for thin sections) and/or using an electric drill (for geochemical and petromagnetic investigations). Amongst the collection, 36 samples were selected for thin section preparation and microscopic investigations of microfacies succession and calpionellid biostratigraphy (following the zonation of Reháková & Michalík, 1997). Additional investigations were made in the Rudnica section, where 30 samples underwent rock magnetic investigations in order to provide additional stratigraphic calibration for the Petrovo Brdo section. The samples were prepared from the same rock fragments as those studied for calpionellid stratigraphy by Reháková and Rožič (2019). Statistical evaluations were performed using JASP Computer Software (2024).

3.1. Paleo- and Rock Magnetism

Paleomagnetic experiments were performed using standard cylindrical specimens (2.2 cm high and 2.5 cm in diameter) which were prepared from drill cores. All the experiments were carried out in the Paleomagnetic Laboratory of the Polish Geological Institute–National Research Institute (PGI–NRI; Warsaw, Poland) in a magnetically shielded space (Magnetic Measurements LFC cage), which reduces the ambient geomagnetic field by ca. 95%. Natural remanent magnetizations (NRM) were measured using Agico JR6A spinner magnetometer and Rema6 software. In order to evaluate magnetostratigraphic potential of the section, 43 specimens from intervals with elevated magnetic susceptibility (19 samples from 0 to 7.5 m interval and 24 samples from 26.5 to 40.6 m) were subjected either to progressive thermal demagnetization (in a Magnetic Measurements MMTD1 thermal demagnetizer) and/or alternating field demagnetization (in a Molspin device, with peak applied field = 100 mT). However, due to the fact that magnetostratigraphic investigations turned out unsuccessful, a detailed description and documentation of paleomagnetic research was put into Supporting Information 1 in https://doi.org/10.5281/zenodo.12542820.

Magnetic susceptibility (MS) was measured both in field and laboratory environments. In the Petrovo Brdo section, field measurements were performed using a ZH Instruments SM30 device with a mean resolution of 25 cm, which accounts for a total of 153 data horizons. Measurements were taken on smooth and perpendicular to the bedding plane surfaces; each horizon was measured three times in order to calculate the mean value. Mass-normalized laboratory MS measurements were processed via Agico MFK1-FB kappabridge and Safyr7 software. Samples coming from all 97 sampled horizons were measured, which accounts for a mean resolution of 40 cm; additional 30 datapoints account for the Rudnica section.

3.2. Stable Isotope Geochemistry

Stable carbon and oxygen isotope analyses were conducted on 99 powder samples using a Gasbench II connected to a ThermoFischer Delta V Plus mass spectrometer at the GeoZentrum Nordbayern (Germany). Oxygen and carbon isotope values are reported in per mil relative to the VPDB scale by calibration to the accepted values of NBS 19 ($\delta^{13}C = +1.95‰$; $\delta^{18}O = -2.20‰$) and LSVEC ($\delta^{13}C = -46.6‰$; $\delta^{18}O = -26.7‰$) references. The reproducibility of the measurements was monitored over the course of analyses by replicated analyses of laboratory standards Erl 5 ($n = 11$), and Sol 2 ($n = 13$). Reproducibility for $\delta^{13}C$ and $\delta^{18}O$ values was 0.05 and 0.03‰ ($\pm 1\sigma$) for Erl 5 as well as 0.05‰, and 0.06‰ ($\pm 1\sigma$) for Sol 2, respectively.

3.3. Total Organic Carbon (TOC)

In order to determine the total organic carbon (TOC) content, Rock-Eval pyrolisys was performed. Measurements were performed on crushed samples using a Vinci Rock-Eval 6 Turbo instrument and IFP 160000 standard at the Polish Geological Institute–National Research Institute, following the method described by Behar et al. (2001). The results included TOC (wt %), hydrogen index (HI, mg HC/g TOC; HC—hydrocarbons), oxygen index (OI, mg CO_2/g TOC) and temperature of maximum hydrocarbon yield (T_{max}, °C) (Espitalié et al., 1985); however, this study utilizes only TOC values.

3.4. Elemental Geochemistry

This study utilizes elemental geochemistry data coming from different analytical methods: gamma ray spectroscopy (GRS), X-ray fluorescence (XRF) and laboratory ICP-ES/MS analyses. Various paleoenvironmental proxies provided an insight into sedimentary conditions prevailing in the area of the Slovenian Basin during the J/K transition; some of them were helpful for stratigraphic correlations.

3.4.1. Field Gamma-Ray Spectroscopy (GRS)

Field gamma-ray spectrometric measurements in the Petrovo Brdo section were carried out using a Georadis GT-32 portable natural radioisotope assay analyzer. 180 s time interval was applied; a vertical step of 50 cm accounts for 80 measurement horizons. Counts per seconds (cps) in selected energy windows were directly converted to concentrations of potassium, K (%), uranium, U (ppm), thorium, Th (ppm) and total dose (nGy/h).

3.4.2. X-Ray Fluorescence (XRF) Measurements

In order to obtain a high-resolution data on concentrations of selected main and trace elements, 94 hand samples were cut, polished and subjected to X-ray fluorescence analyses using the Thermo Fischer NITON handheld device (University of Ljubljana, Slovenia). In case of 54 samples, two or more measurements were performed, so that their average values are used.

3.4.3. ICP-MS Analyses

In order to evaluate accuracy and credibility of portable XRF measurements, a set of 16 selected samples was intended for additional ICP-ES/MS analyses following near-total acid digestion (LF 200 procedure) in the Bureau Veritas Ltd. Major elements were detected with accuracy below 0.01% (except 0.04% for Fe and 0.002% for Cr), whereas for most of trace elements (Cu, Mo, Ni, Pb, Rb, U, Zn, Zr) accuracy was 0.1 ppm (except Th—0.2 ppm, as well as Ba and Zn—1 ppm).

3.4.4. Geochemical Proxies

Due to its low diagenetic mobility, lithogenic input to the Slovenian Basin was estimated primarily based on Al concentrations. Besides, the total amount of terrigenous input was approximated using a computed gamma ray index (CGR) using the following formula: CGR [API] = 3.93 × Th [ppm] + 16.32 × K [%] (Kumpan et al., 2014; Rider, 1990).

Paleoclimate signals were evaluated herein based on humidity-related potassium proxies, such as Th/K (Ruffel & Worden, 2000), Al/K (Wei et al., 2006) and Ti/K (Arnaud et al., 2012). These ratios reflect differential chemical leaching of K relative to Th, Al, and Ti. Material subjected to erosion, transportation and deposition in sedimentary basins is relatively impoverished in K and manifests as relatively elevated Ti/K, Al/K, and Th/K. These

proxies were successfully applied in the Tithonian–Berriasian sedimentary successions of variegated paleogeographic settings (Grabowski, Chmielewski, et al., 2021; Lodowski & Grabowski, 2023; Schnyder et al., 2006). In order to estimate the transport energy and possible grain-size variations and/or density fractionation, Zr/Al and Ti/Al ratios were calculated (Calvert & Pedersen, 2007; Schnetger et al., 2000).

To investigate whether the sediments were subjected to oxygen depletion, various authors usually adopt the authigenic U formula of Jones and Manning (1994). However, the original formula relies on U/Th ratio in the Kimmeridge Clay and therefore is formation specific; in turn, in the Petrovo Brdo section, mean U/Th is 5.09 ± 2.39. Consequently, for the purposes of this study authigenic U is approximated using modified formula: Authigenic $U = U_{SAMPLE} - \frac{Th_{SAMPLE}}{4.5}$. Additionally, Fe/Al ratio (Algeo & Liu, 2020) was also calculated.

Enrichment factors (EF $X = \frac{\frac{X_{SAMPLE}}{Al_{SAMPLE}}}{\frac{X_{AVERAGE\ SHALE}}{Al_{AVERAGE\ SHALE}}}$, where X is the element considered; Li & Schoonmaker, 2003) were calculated for selected trace metals (Ba, Cu, Zn), which are known for their importance to living organisms and/or nutrient-type distribution in sediments (Tribovillard et al., 2006). Along with biological ("excess") concentrations, they are primarily considered in the context of paleoproductivity and changes in uptake (water-mixing) processes (see Grabowski, Stoykova, et al., 2021; Lodowski & Grabowski, 2023). Biological fluxes were approximated using the equation of Shen et al. (2015): $X_{EXCESS} = X_{SAMPLE} - (Al_{SAMPLE} \times D)$, where X is the examined element while D is a "detrital" constant, approximated as the lowest non-protruding *X/Al* ratio in the entire data set (see also Lodowski & Grabowski, 2023).

4. Results

4.1. Microfacies Succession

In thin sections, radiolarian cherts of the Tolmin Formation are made of microcrystalline silica with dispersed (wackestone-type) radiolarians and sponge spicules. Although radiolarians are common, they are not rock-forming (Figures 3.1 and 3.2).

Microfacies of the subsequent Biancone Limestone Formation are rather uniform and are dominated by mudstones and wackestones. These are often laminated and sporadically bioturbated; intraclasts also occur and are almost exclusively pelagic bioclasts (Figures 3.3–3.5). The most common are calcified radiolarians and sponge spicules; calpionellids are very rare and are found almost solely within the lower part of the formation. Other rare bioclasts are calcareous dinoflagellate cysts, ostracods, aptychi, echinoderm plates, and foraminifera (*Spirillina* sp.).

Matrix of the Biancone Limestone is micrite, often recrystallized to microspar. Within the lower part of the section, between meters 8 and 10, thin sections document the presence of framboidal pyrite (Figure 3.3). Patches and stripes made of dispersed microcrystalline quartz and/or slightly coarser (up to 100 μm) and more concentrated irregular quartz crystals document silicification; this phenomenon is most common within the middle part of the formation, where chert nodules also occur (see Figure 2). Dissolution seams, which are parallel to bedding and lamination, are most common within the upper part of the Biancone Limestone; besides, thin sections are usually cut by calcite veins.

4.2. Biostratigraphy

Calpionellids in the Petrovo Brdo section are rare and poorly preserved; therefore, only some index species were determined. The lower part of the Biancone Limestone Formation (5.2–20.8 m of section) contains cysts of *Colomisphaera carpathica*, *Colomisphaera lapidosa*, *Stomiosphaera moluccana* as well as very rare hyaline loricae of *Calpionella alpina*, *Calpionella grandalpina*, *Calpionella elliptalpina*, *Crassicollaria parvula*, *Crassicollaria massutiniana* and *Tintinnopsella carpathica*, therefore association which is typical for the upper Tithonian Crassicollaria Zone (Figures 2 and 3.6).

In the upper part of the Biancone Limestone Formation (between meter 20.8 and 24.1) small forms of *Calpionella alpina* occur, what suggests the presence of the Calpionella alpina Subzone. Besides, oblique sections of calpionellid loricae and several cysts of *Colomisphaera lapidosa* and *Stomiosphaera moluccana* (Figure 3.6) were documented. Above meter 24.1 calpionellids almost disappear; few loricae of *Calpionella alpina* were observed only in sample PB39.5 near the top of the section.

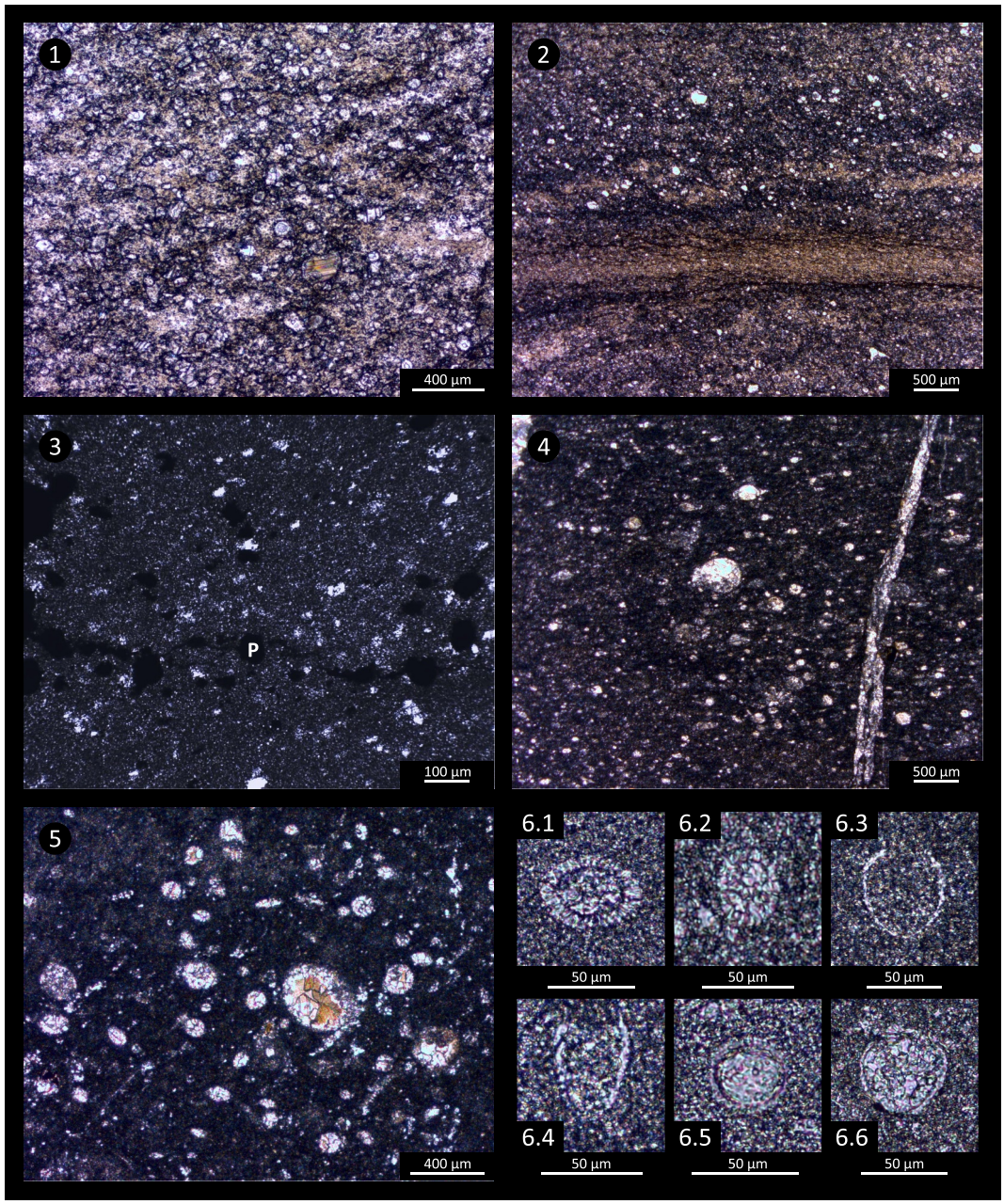

Figure 3. Microfacies (1–5) and selected microfossils (6) of the Petrovo Brdo section. 1, 2—sponges and radiolarians of the 'radiolarite' Tolmin Fm. (1: sample PB-0; 2: PB-2.9); 3—pyrite framboids (P) within the Biancone Limestone Fm. (PB-8.0); 4—sponge spicules in Biancone limestone (PB-26); 5—radiolarians in Biancone limestone (PB-37.5); 6.1—*Colomisphaera carpathica* (PB-7.0); 6.2—*Colomisphaera lapidosa* (PB-8.0); 6.3—*Calpionella grandalpina* (PB-8.8); 6.4—*Crassicollaria parvula* (PB-13); 6.5—*Stomiosphaera moluccana* (PB-20); 6.6—*Calpionella alpina* (PB-39.5).

Due to lack of microfossil control, the boundary between the Tolmin and the Biancone Limestone Formation cannot be dated in the Petrovo Brdo section. However, the regional stratigraphy of this interval is well constrained (Goričan, Pavšič, & Rožič, 2012; Goričan, Kosir, & Rožič, 2012; Rožič, 2009), which allows to approximate the lithological boundary to the lower/upper Tithonian transition (see chapter 5.1. "Biostratigraphic calibration"). Besides, the late Tithonian age of the onset of BL Fm. is assessed for the entire Selška Sora Valley (Demšar, 2016).

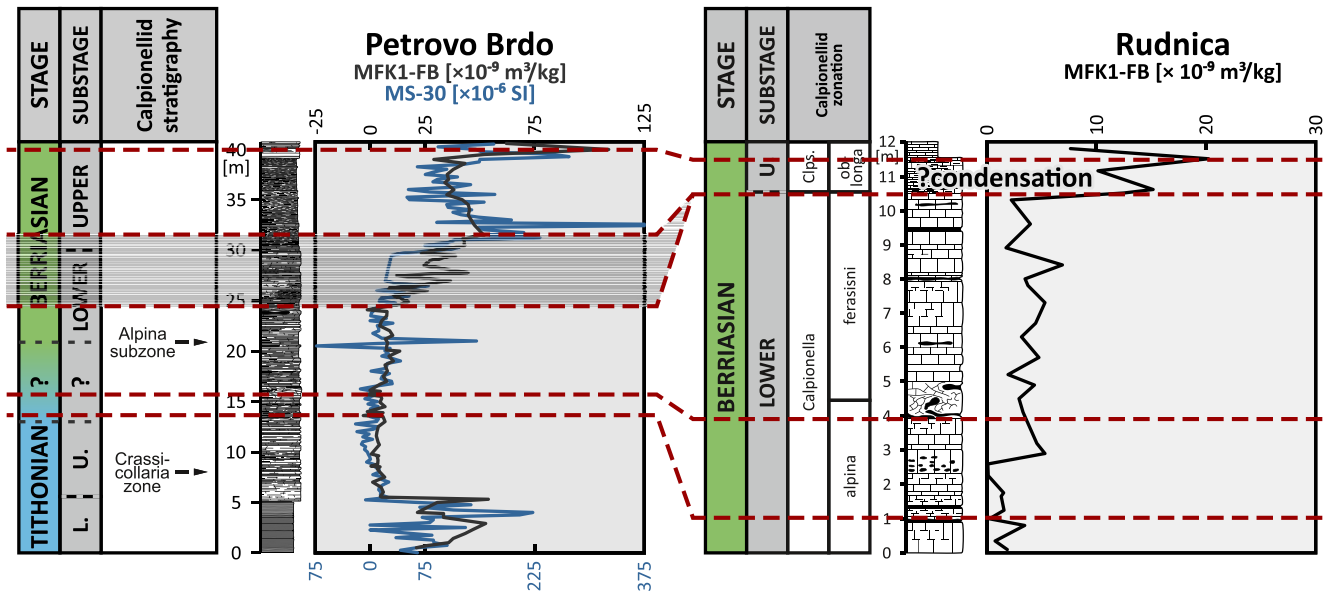

Figure 4. Correlation of magnetic susceptibility between the Petrovo Brdo and Rudnica sections. Abbreviations: L.—lower; U.—Upper; Clp.—Calpionellopsis. Correlation of the upper Berriasian is based on trends in magnetic susceptibility; in the Tithonian–Berriasian boundary interval, correlation is based upon the occurrence of slump and chert levels.

4.3. Magnetic Susceptibility

Both field and laboratory measured MS measurements performed in the Petrovo Brdo section document concordant trends (Figure 4). The basal part of the section (Tolmin Fm., 0–5 m) is characterized by a relatively strong MS signal (20–55 $\times$ 10^{-9} m^3/kg). It falls to near-zero values at meter 5, along with the onset of the Biancone Limestone Formation, and remains very low or even negative (cf. 10–15 m) up to meter 25. Above, a sudden increase in MS (up to 55 $\times$ 10^{-9} m^3/kg) characterizes the interval of meters 25–32; although within subsequent beds (32–38 m) MS slightly decreases, another peak marks the top of the section (109 $\times$ 10^{-9} m^3/kg).

In the case of the Rudnica section, minimal MS accounts for the bottom 2.5 m of the section (ca. 1.5 $\times$ 10^{-9} m^3/kg). Above, it becomes slightly elevated (ca. 4 $\times$ 10^{-9} m^3/kg) within the upper part of the Alpina and the Ferasini calpionellid subzones (2.5–10.5 m). Finally, the top of the section (Oblonga Subzone; 10.5–12 m) is characterized by an increase in MS, up to 20 $\times$ 10^{-9} m^3/kg (Figure 4).

4.4. Stable Carbon and Oxygen Isotopes

In the Petrovo Brdo section, stable carbon isotopic ratios vary between 0.55 and 2.16 ‰ VPDB, revealing an overall decreasing trend. The basal 15 m of the section clearly documents the descending trend (down to ca. 1.25‰), with the Tolmin/Biancone Limestone formational boundary being marked by an additional and local $\delta^{13}C$ drop. Above (15–30 m), the carbon isotope curve fluctuates between 1.15 and 1.45‰ to increase notably (to ca. 1.7‰) at meter 30. Finally, the upper part of the section (30–40.6 m) is characterized by another decreasing trend; noteworthy, the topmost 3 m of the section (above meter 38) account for a rapid fall of $\delta^{13}C$ values (from 1.26 to 0.55; Figure 5).

$\delta^{18}O$ varies between −2.92 and −6.78‰ and may be divided into two segments that document distinct trends. The basal 10 m of the section accounts for generally increasing values (from ca. −4 to −3 ‰), with the trend being interrupted by a local drop to −5.4 ‰ at the boundary between the Tolmin and the Biancone Limestone formations (marly layer at meter 5). Above, a prolonged decreasing trend continues up to the top of the section; however, it is less pronounced within the lower part of the interval (meters 10–20), whereas a sudden drop marks the level of meter 25. No significant statistical correlations between carbon and oxygen isotope ratios occur in the entire section (Figure 5); however, a moderate positive correlation is observed in the upper part of the section between meters 32.5 and 40.6 m (Pearson's $r = 0.73$, $p < 0.001$, $n = 17$).

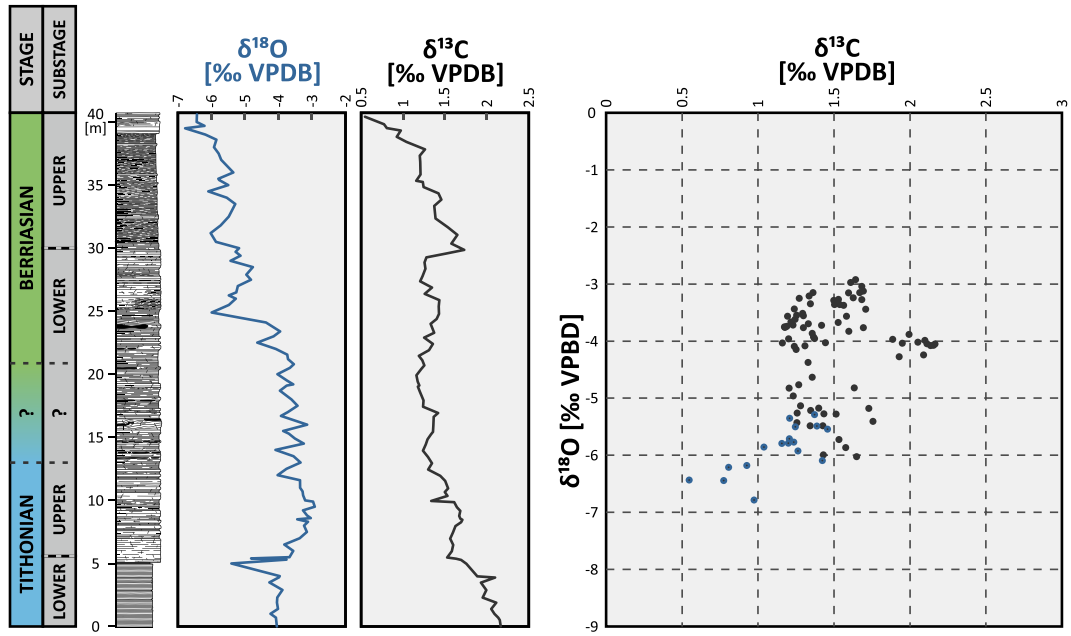

Figure 5. Stable oxygen and carbon isotopes in the Petrovo Brdo section (left). A cross-plot of $\delta^{13}C$ and $\delta^{13}O$ is shown on the right. Blue dots indicate ratios in the topmost 8 m of the section (32.5–40.6 m).

4.5. Geochemistry

4.5.1. Comparison of Laboratory Data (ICP-ES/MS) With Gamma Ray Spectrometry (GRS) and Portable X-Ray Fluorescence (pXRF) Measurements

Laboratory analyses (ICP-ES/MS) show that the Petrovo Brdo section accounts for considerable variations in Al content (0.27%–4.29%; see Supporting Information 2 in https://doi.org/10.5281/zenodo.12542820), with the highest concentrations at its base (Tolmin Fm.; 0–5 m; 2.48%–4.29%). At the base of the Biancone Limestone Formation (sample PB5.5), Al concentration drops to 0.27%; such low and generally stable values occur up to the meter 25. Above this horizon, Al content increases from 0.71% (sample PB24.1) to 2.34% (sample PB33.5). At the top of the section, Al concentration remains generally elevated, yet in sample PB38.6 a local low (1.1% Al) is observed. Concentrations of Ti, Zr, Th, K, Rb, U, Mg, Co and Fe ($0.90 < r < 1$; for all $p < 0.001$, $n = 16$) as well as Na, Si, P, Cu and Zn ($0.8 < r < 0.9$; for all $p < 0.001$, $n = 16$) are strongly correlated to the concentration of Al, indicating their detrital provenance. Considered as only partially detrital are Ni ($r = 0.65$, $p = 0.006$, $n = 16$) and Ba ($r = 0.53$, $p = 0.034$, $n = 16$), whereas Mn is affiliated to authigenic (non-detrital) phases ($r = 0$, $p = 0.998$, $n = 16$). Calcium, which is the most common element within the data set (4.9%–37.9%, median = 30.3%), reveals strong negative correlation with Al ($r = -0.92$, $p < 0.001$, $n = 16$), and therefore is regarded as related to carbonate matrix (Table 1).

Both GRS and XRF measured content of K, U, and Th follow the trends documented by laboratory analysis; however, elemental concentrations measured by portable devices are systematically higher than those obtained using ICP-MS (Figure 6; see also Supporting Information 2 in https://doi.org/10.5281/zenodo.12542820), which translates into higher CGR indexes. Contents of K, Th and values of the CGR index are more concordant between GRS and ICP-MS data than with handheld XRF. Ultimately, ICP-MS and GRS methods also provide a consistent measurements of U, Th and K content ($r = 0.79$, 0.87, and 0.78, respectively; for all $p < 0.001$, $n = 16$).

Portable XRF measured content of Al, Ti, Zr, K, Rb, Fe, Ni, Si, and Ca remains in agreement with ICP-MS data (for all elements $r > 0.85$, $p < 0.001$, $n = 16$). Good correlation between data sets occurs for Zn ($r = 0.78$, $p = 0.001$, $n = 16$) and Th ($r = 0.74$, $p = 0.001$, $n = 16$), whereas only moderate correlation occurs for Cu ($r = 0.65$, $p = 0.007$, $n = 16$). Noteworthy, in the case of Ni and Ba, their pXRF concentrations are much higher than those of ICP-MS. In general, the geochemical contrast between the Tolmin and Biancone formations in pXRF is more poorly expressed.

Geochemistry, Geophysics, Geosystems

10.1029/2024GC011728

Table 1

Pearson Correlation Coefficients (PCC) and Coefficients of Deteremination (R^2) of Laboratory ICP-MS (a) and Portable XRF (b) Measured Concentrations of Selected Chemical Elements, Stable Carbon ($\delta^{13}C$) and Oxygen ($\delta^{18}O$) Isotopes, and Magnetic Susceptibility (MS)

(a)

ICP-MS																								
PEARSON CORRELATION COEFFICIENT (r)	Al	1.00																						
	Ti	**0.99**	1.00																					
	Zr	**0.98**	**0.97**	1.00																				
	Th	**0.98**	**0.95**	**0.98**	1.00																			
	K	**0.98**	**0.95**	**0.97**	**0.99**	1.00																		
	Rb	**0.98**	**0.95**	**0.97**	**0.98**	**1.00**	1.00																	
	U	**0.97**	**0.97**	**0.96**	**0.94**	**0.92**	**0.92**	1.00																
	Mg	**0.95**	**0.97**	**0.91**	0.87	0.89	0.89	**0.91**	1.00															
	Co	**0.94**	**0.94**	**0.94**	**0.91**	0.89	0.90	**0.91**	**0.91**	1.00														
	Fe	**0.92**	**0.94**	0.89	0.84	0.85	0.85	**0.90**	**0.95**	**0.92**	1.00													
	Na	0.89	**0.92**	0.87	0.82	0.79	0.79	**0.94**	**0.91**	0.84	0.88	1.00												
	Si	0.87	0.83	0.90	**0.92**	0.88	0.89	0.82	0.74	**0.92**	0.75	0.68	1.00											
	P	0.87	0.87	0.85	0.85	0.83	0.83	0.82	0.84	0.89	0.87	0.80	0.83	1.00										
	Cu	0.83	0.84	0.79	0.80	0.81	0.81	0.79	0.85	0.84	0.73	0.72	0.77	0.75	1.00									
	Zn	0.80	0.84	0.77	0.73	0.71	0.72	0.82	0.88	0.85	0.85	0.86	0.70	0.78	0.84	1.00								
	Ni	0.65	0.72	0.61	0.51	0.50	0.50	0.69	0.77	0.71	0.85	0.82	0.43	0.67	0.50	0.75	1.00							
	Ba	0.53	0.60	0.44	0.37	0.47	0.47	0.50	0.72	0.46	0.70	0.57	0.16	0.48	0.47	0.57	0.71	1.00						
	Mn	0.00	0.09	0.01	-0.14	-0.12	-0.12	0.15	0.20	0.07	0.28	0.29	-0.15	0.02	0.03	0.38	0.48	0.36	1.00					
	Ca	**-0.92**	-0.89	**-0.93**	**-0.95**	**-0.92**	**-0.93**	-0.87	-0.80	**-0.95**	-0.81	-0.74	**-0.99**	-0.86	-0.80	-0.75	-0.49	-0.25	0.10	1.00				
	$\delta^{13}C$	0.36	0.28	0.40	0.47	0.49	0.49	0.28	0.18	0.22	0.05	0.04	0.42	0.16	0.34	-0.06	-0.35	-0.12	-0.52	-0.40	1.00			
	$\delta^{18}O$	-0.49	-0.56	-0.45	-0.35	-0.37	-0.37	-0.51	-0.67	-0.59	-0.71	-0.64	-0.37	-0.62	-0.57	-0.80	-0.80	-0.64	-0.63	0.43	0.39	1.00		
	MS	0.89	**0.92**	0.87	0.80	0.81	0.82	0.87	**0.93**	**0.94**	**0.98**	0.86	0.78	0.87	0.77	0.88	0.85	0.67	0.31	-0.83	0.04	-0.78	1.00	
		Al	Ti	Zr	Th	K	Rb	U	Mg	Co	Fe	Na	Si	P	Cu	Zn	Ni	Ba	Mn	Ca	$\delta^{13}C$	$\delta^{18}O$	MS

Geochemistry, Geophysics, Geosystems

10.1029/2024GC011728

Table 1
Continued

(b)

XRF		Al	Ti	Zr	K	Rb	Fe	Zn	Ni	Mg	Ba	Th	Si	Cu	Mn	Co	Ca	$\delta^{13}C$	$\delta^{18}O$	MS
PEARSON CORRELATION COEFFICIENT (r)	Al	1.00																		
	Ti	**0.98**	1.00																	
	Zr	**0.99**	**0.98**	1.00																
	K	**0.97**	**0.97**	**0.96**	1.00															
	Rb	**0.97**	**0.96**	**0.97**	**0.99**	1.00														
	Fe	**0.94**	**0.94**	**0.94**	**0.90**	**0.91**	1.00													
	Zn	0.82	0.85	0.81	0.82	0.78	0.80	1.00												
	Ni	0.72	0.77	0.70	0.71	0.64	0.75	0.80	1.00											
	Mg	0.65	0.70	0.62	0.70	0.61	0.65	0.79	0.75	1.00										
	Ba	0.60	0.66	0.57	0.67	0.57	0.59	0.68	0.81	0.80	1.00									
	Th	0.68	0.68	0.65	0.69	0.66	0.59	0.62	0.52	0.61	0.57	1.00								
	Si	0.54	0.48	0.58	0.45	0.57	0.54	0.22	0.03	-0.15	-0.22	0.12	1.00							
	Cu	0.34	0.35	0.36	0.31	0.31	0.36	0.27	0.31	0.22	0.16	0.08	0.25	1.00						
	Mn	0.35	0.39	0.33	0.29	0.24	0.47	0.47	0.56	0.37	0.39	0.22	-0.02	0.30	1.00					
	Co	-0.52	-0.53	-0.54	-0.47	-0.49	-0.56	-0.32	-0.35	-0.15	-0.21	-0.23	-0.45	-0.15	-0.35	1.00				
	Ca	-0.64	-0.59	-0.68	-0.56	-0.67	-0.63	-0.31	-0.16	0.03	0.09	-0.17	**-0.98**	-0.28	-0.03	0.50	1.00			
	$\delta^{13}C$	0.11	0.03	0.11	0.06	0.14	-0.03	-0.05	-0.36	-0.21	-0.44	0.11	0.48	0.08	-0.36	0.01	-0.39	1.00		
	$\delta^{18}O$	-0.63	-0.66	-0.64	-0.60	-0.58	-0.75	-0.61	-0.69	-0.47	-0.49	-0.25	-0.32	-0.30	-0.69	0.50	0.43	0.39	1.00	
	MS	0.73	0.73	0.74	0.65	0.67	0.84	0.60	0.62	0.40	0.34	0.35	0.54	0.34	0.60	-0.50	-0.58	-0.11	-0.75	1.00
		Al	Ti	Zr	K	Rb	Fe	Zn	Ni	Mg	Ba	Th	Si	Cu	Mn	Co	Ca	$\delta^{13}C$	$\delta^{18}O$	MS
		PEARSON CORRELATION COEFFICIENT (r)																		

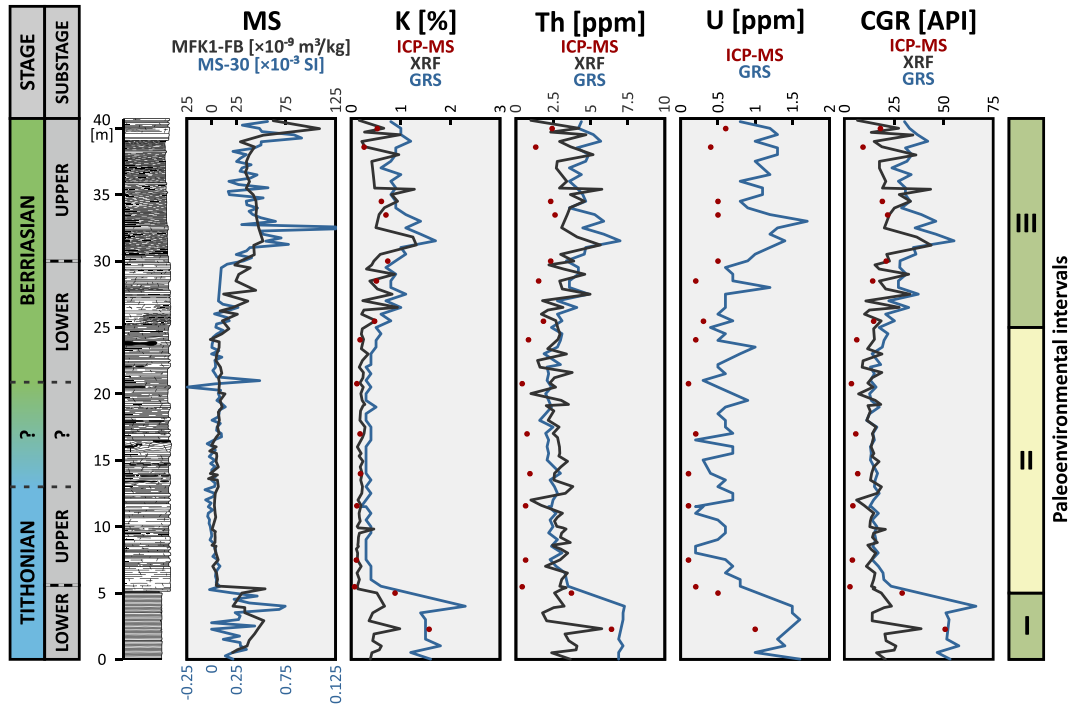

Figure 6. Field and laboratory measured magnetic susceptibility in the Petrovo Brdo section as well as K, Th, U, and CGR values obtained using different methods (laboratory ICP-MS, portable XRF and field GRS measurements).

The relative carbonate content (Ca/Al) documents reversed trends in relation to CGR ($r_{XRF} = -0.73$; $r_{ICP\text{-}MS} = -0.79$), with low carbonate content (=high terrigenous admixture) in the Tolmin Formation (basal 5 m), high carbonate (=low terrigenous) within the lower part of the Biancone Limestone Formation (ca. up to meter 25) and—again—low carbonate within the upper part of the BL Fm. (above meter 25). Silicon, the second most abundant element in the studied section (1.3%–32%, median ca. 7.5%), shows consistent concentrations from both pXRF and laboratory measurements ($r = 0.99$, $p < 0.001$, $n = 16$). These basically mirror the Ca content (both r_{pXRF} and $r_{ICP\text{-}MS} = -0.99$, $p < 0.001$, $n = 16$) and are in negative phase to Ca/Al ($r_{XRF} = -0.73$, $p = 0.001$, $n = 16$; $r_{ICP\text{-}MS} = -0.66$, $n = 0.005$, $n = 16$). The content of Si generally follows the terrigenous curves (for Si vs. other detrita elements $0.75 < r < 1$, $p < 0.001$, $n = 16$), revealing the highest values in the Tolmin Fm. However, some unrelated terrigenous element Si spikes are also observed. Elevated values of the Si/Al ratio characterize the Tolmin Fm. as well as several horizons within the middle part of the section, indicatory of authigenic silica. The Si/Al spikes match well the negative shifts of Ca and Ca/Al curves (see Supporting Information 2 and 3 in https://doi.org/10.5281/zenodo.12542820).

Statistical comparison of paleoclimate related terrigenous elemental ratios (Ti/K, Al/K, Th/K, Ti/Al, Zr/Rb) calculated from ICP-MS and pXRF data sets reveal only moderate correlation (see Figure 8 and Supporting Information 3 in https://doi.org/10.5281/zenodo.12542820). For the Ti/Al ratio, both methods document similar trends (a slight decrease up to meter 14 and a consecutive increase above) when reject anomalous PB11.6 record ($r = 0.63$ vs. $r = 0.72$). Trends in the Al/K ratio follow the Ti/Al curve, yet in this case field measured values correlate well with laboratory data. The Zr based ratios (Zr/Rb and Zr/Al) are strongly discordant between 5 and 15 m of the section, whereas correlation upsection is much better. Above meter 30, the Ti/K ratio reveals an increase in both pXRF and ICP-MS data sets. The Th/K ratio increases at the base of the Biancone Limestone (5 and 6 m) and generally decreases above; ICP-MS data correlate better with GRS than the pXRF data set. On this basis, the most reliable portion of the section for paleoclimate considerations is regarded as the interval above meter 15.

Since U was not documented using the pXRF method, the record of U-based proxies can be compared only between GRS and ICP-MS data. Authigenic U correlates quite well between the data sets ($r = 0.51$, $p = 0.047$, $n = 16$), whereas the correlation in U/Th is weak ($r = 0.38$, $p = 0.146$, $n = 16$). However, when high-resolution

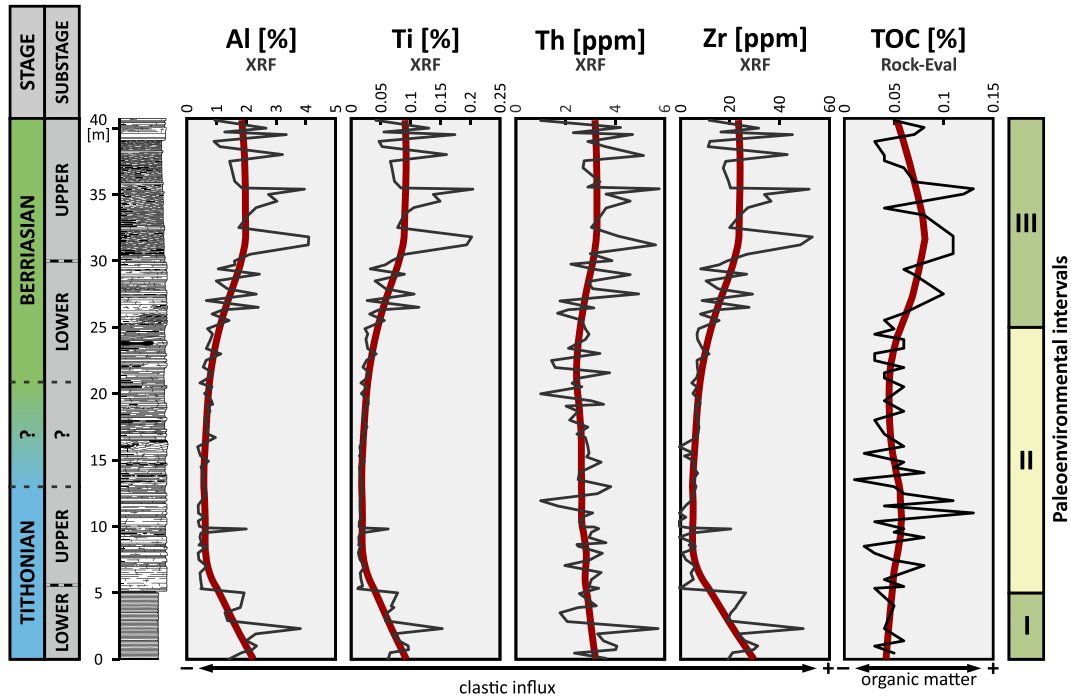

Figure 7. Detrital elements and TOC content in the Petrovo Brdo section. Thick red lines indicate represent 35% LOWESS regression smoothed curves.

GRS U data are compared, authigenic U and U/Th correspond to each other ($r = 0.94$, $p < 0.001$, $n = 80$). The ratio of Fe/Al does not correlate with U-based proxies; therefore, it is unlikely that it reflects paleoredox conditions in this case.

When enrichment factors and 'excess' values of Ba, Zn and Cu are considered, they document similar trends, and these trends are coherent in both the pXRF and ICP-MS data sets (for all $r > 0.80$, $p < 0.001$, $n = 16$; Supporting Information 3 in https://doi.org/10.5281/zenodo.12542820).

4.5.2. High Resolution (pXRF and GRS) Geochemical Measurements

The basal 5 m of the section (Tolmin Formation) is relatively rich in terrigenous elements (i.e., Al). Their concentrations decrease at the base of the Biancone Limestone Formation (meter 5) and remain low above, however a gentle, increasing trend occurs above meter 15. Nonetheless, the relative share of lithogenic elements increases clearly only above meter 25; the topmost 10 m of the section (36–41 m) account for their highest yet variable concentrations (Figure 7).

Changes in terrigenous flux apparently correlate with the composition of terrigenous fraction (Figure 8; Supporting Information 3 in https://doi.org/10.5281/zenodo.12542820). The upper part of the section, above meter 28 m, is relatively enriched in Ti (high Ti/Al and Ti/K) and Zr (elevated Zr/Rb and Zr/Al), as well as depleted in K (relatively high Al/K and Ti/K). The middle interval (15–25 m), in turn, is relatively rich in K (low Al/K) and depleted in Ti and Zr (profound low Ti/Al, slightly lowering Zr/Rb and Zr/Al). Data from the basal part of the section are the least reliable (see above); however, they point to K (elevated Al/K) and Ti (high Ti/Al) enrichment. Despite the lower quality of data, the Ti/K and Zr/Al (Zr/Rb) curves suggest Ti and Zr enrichment and depletion in K.

Surprisingly, the Th/K curve does not follow the trends in detrital ratios, revealing rather an affinity to trace metal enrichment and their excess fractions (i.e., Cu, Zn), with a large contrast at the boundary between Tolmin and Biancone Limestone formations, generally decreasing trend above, and a slight elevation at the top of the section (compare Figures 8 and 9 with Supporting Information 3 in https://doi.org/10.5281/zenodo.12542819).

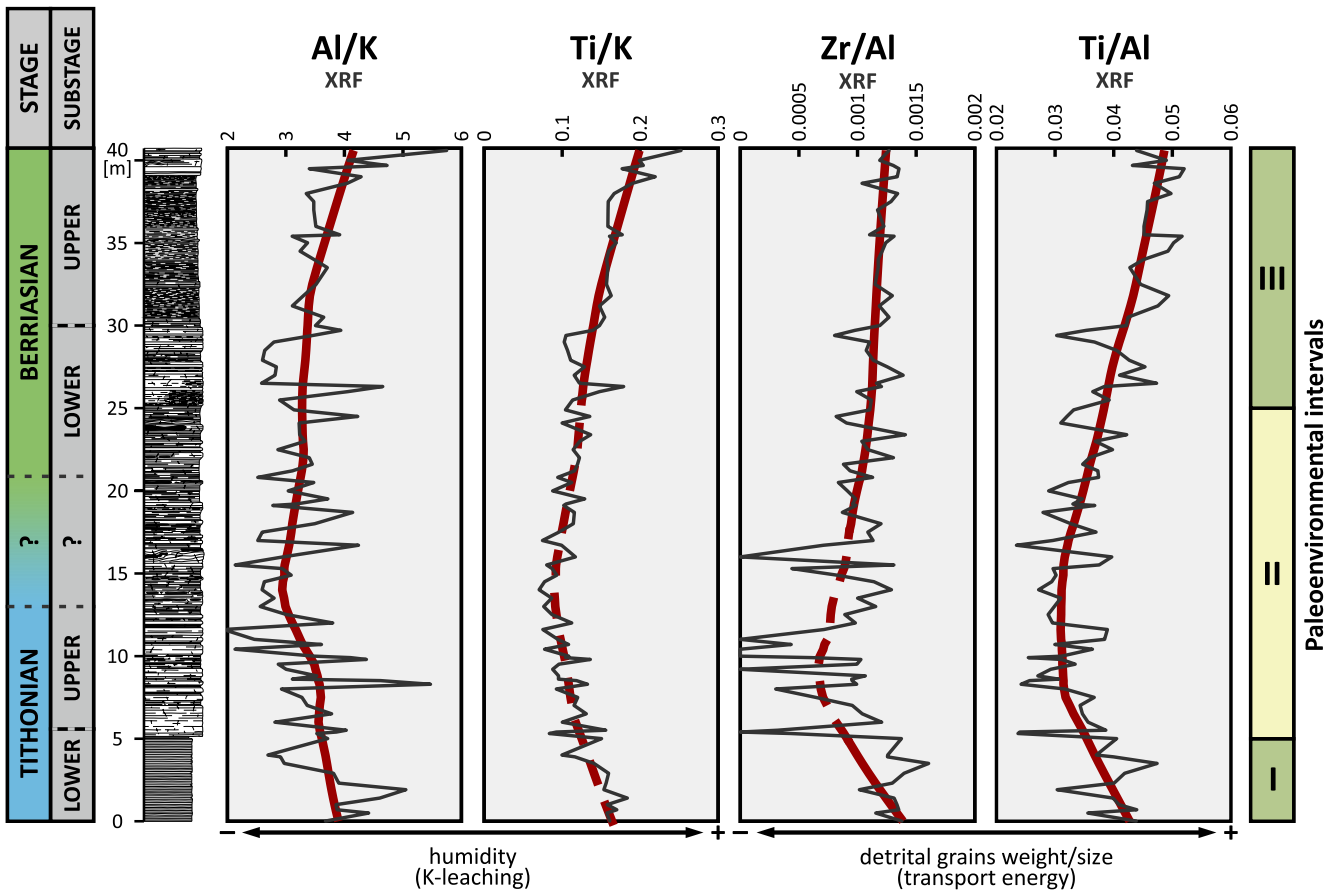

Figure 8. Selected paleoclimate proxies in the Petrovo Brdo section. Thick red lines indicate represent 35% LOWESS regression smoothed curves; dashed lines indicate intervals with poor correlation between the ICP-MS and pXRF data sets.

Both authigenic U and U/Th (GRS measured) are characterized by an increasing trend from the base of the section up to ca. meter 20, a slight decrease above, and another slightly increasing trend from ca. meter 25 up to the top of the section (Figure 9; Supporting Information 3 in https://doi.org/10.5281/zenodo.12542820).

Either EF and "excess" values of nutrient-type trace elements (Ba, Cu, Zn) document similar trends with only minor differences. The basal 5 m (Tolmin Formation) account for the relatively lowest values of those indices, which increase notably at the base of the Biancone Limestone Formation (near meter 5). The successive Biancone Limestone Formation documents decreasing values of EFs of Ba, Cu and Zn up to meter 30 as well as low and rather stable values within the topmost 10 m of the section. In turn, "excess" fractions of Ba, Cu and Zn remain high and stable up to meter 25 and decrease slightly above, within 25–30 m intervals, similar to trends documented in authigenic U and U/Th (Figure 9; Supporting Information 3 in https://doi.org/10.5281/zenodo.12542820). Here it must be also noted that due to strong detrital affinities of the element Zn (Table 1), a relatively strong "detrital offset" was adopted in case of Zn_{EXCESS} calculation.

4.5.3. TOC Content

In general, total organic carbon content in the Petrovo Brdo is very low, usually ca. 0.05% of rock mass. However, there are two intervals, where TOC is slightly enriched, exceeding 0.1%: (a) within the upper Tithonian (around meter 10); and (b) at the lower/upper Berriasian transition (25–35 m) (Figure 7). In general, TOC content correlates with Al only limitedly ($r = 0.41$, $p < 0.001$, $n = 63$). However, when considering the Berriasian interval (cf. above meter 15) this relation becomes statistically significant ($r = 0.70$, $p < 0.001$, $n = 38$), suggesting predominantly detrital origins of organic carbon in the upper part of the section. In order to estimate the amount of "authigenic" (non-detrital) organic carbon, a TOC/Al ratio has been calculated. It is characterized by low values within the Tolmin Formation (cf. lower Tithonian), significantly elevated values within the lower part of the

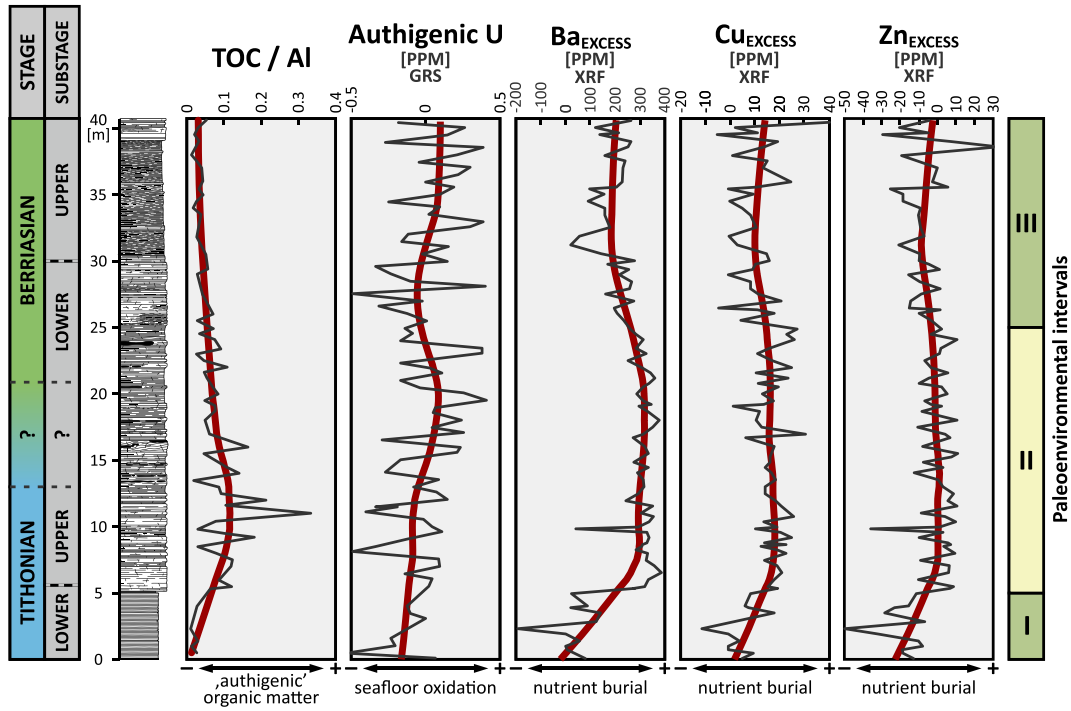

Figure 9. TOC/Al, authigenic U and selected nutrient-type trace metals (their biogenic fractions) in the Petrovo Brdo section. Thick red lines indicate represent 35% LOWESS regression smoothed curves.

Biancone Limestone (upper Tithonian–? lowermost Berriasian; ca. 5–15 m), and again low values in the upper part of the section (Figure 9).

5. Interpretation

5.1. Stratigraphic Callibration

Despite poor biostratigraphic dating, the chronostratigraphic framework of the Petrovo Brdo section can be established. The boundary between the Tolmin and the Biancone Fm. falls close to the lower/upper Tithonian boundary (Goričan, Pavšič, & Rožič, 2012; Goričan, Kosir, & Rožič, 2012). The topmost part of the Tolmin Fm. belongs to the UAZ 12 Radiolarian Zone, which corresponds to early–early late Tithonian (Goričan et al., 2018). Basal beds of the Biancone Limestone Fm. yield calcareous nannofossils, which are characteristic of the Nannofossil Calcification Event (NCE I) of Bornemann et al. (2003) (Goričan, Pavšič, & Rožič, 2012; Goričan, Kosir, & Rožič, 2012). The event was originally placed between NJK-A and NJK-B calcareous nannofossil subzones *sensu* Bralower et al. (1989; within magnetozone M20n); later on Casellato and Erba (2021) approximated it to the NJT16/NJT17 nannozonal transition. However, the exact placement of the first NCE event against magnetostratigraphy is disputable; it may be situated either within the upper part of M20n1n (NJT 16–NJT 17 nannozonal boundary; Grabowski et al., 2019) or slightly lower between M20r and M20n2n (mostly within NJT 16 nannozone; Lodowski et al., 2022). In this context, the presence of *Crassicollaria* sp. near the base of the Biancone Fm. (Figure 2) suggests that this interval corresponds to Crassicollaria calpionellid Zone, usually correlated with upper M20n–lower M19n2n (Lodowski et al., 2022). Consequently, the base of the Biancone Limestone in the Petrovo Brdo section most likely corresponds to magnetozone M20n (lower upper Tithonian), whereas the topmost part of the Tolmin Fm., along with a marly layer between the Tolmin and BL Fm., may be of the late early Tithonian age (?coeval to M20r). Finally, the existence of a gap or a condensed interval at the boundary between the Tolmin and Biancone formations, as suggested by a sharp contrast in various paleoenvironmental proxies between the formations, cannot be excluded (Figures 6–10).

The Tithonian–Berriasian boundary can be placed not higher than 20.0–20.8 m interval, where a small form of *Calpionella alpina* appears. One of the characteristic features of the Petrovo Brdo section is a sedimentary slump at the 16 m horizon (Figure 2). Even though it falls below the first occurrence of small *Calpionella alpina*, its late

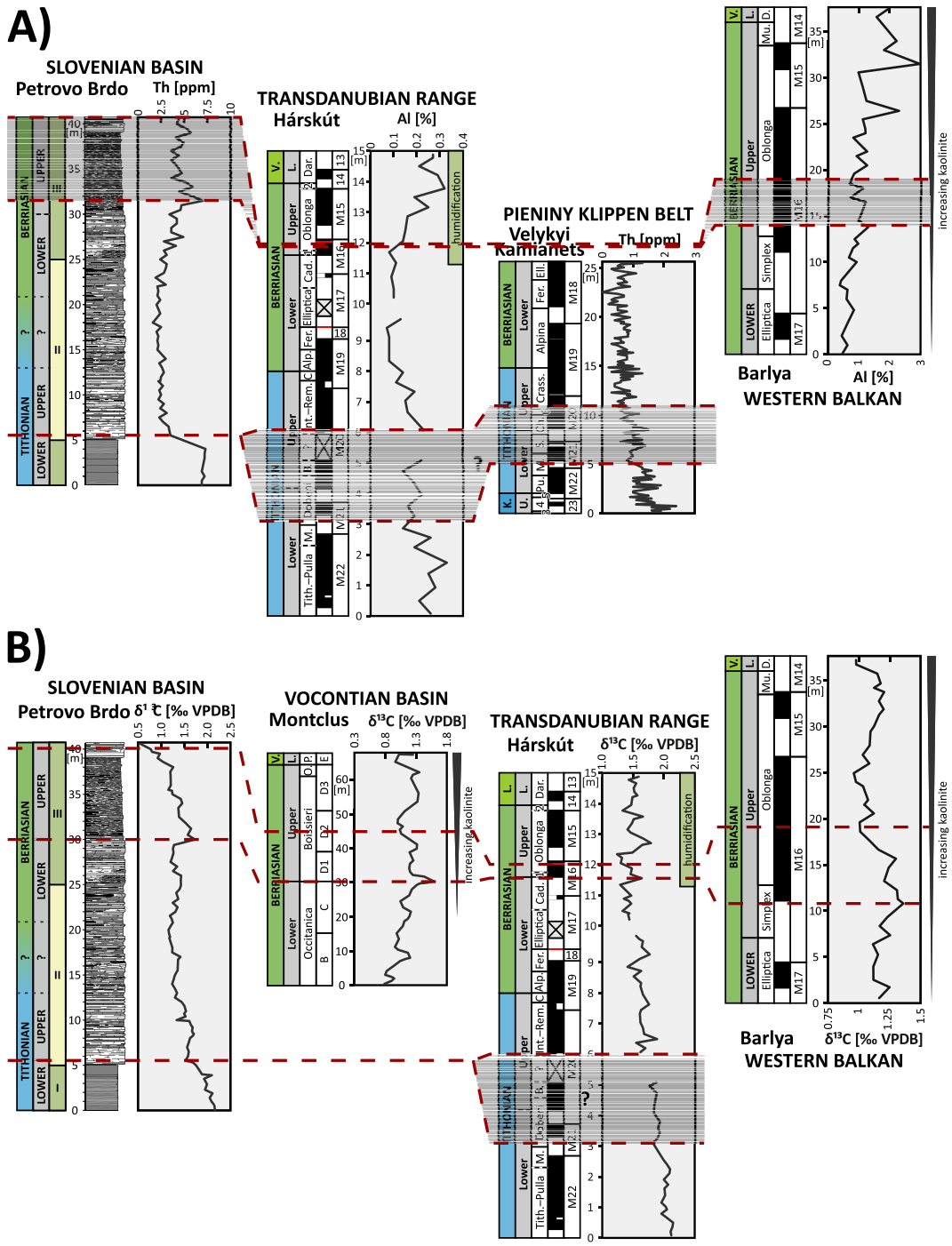

Figure 10. (a) Correlation of terrigenous influx in the Petrovo Brdo (this study), Hárskút (Lodowski et al., 2024), Velykyi Kamianets (Grabowski et al., 2019) and Barlya (Grabowski, Stoykova, et al., 2021) sections. (b) $\delta^{13}C$ correlation between the Petrovo Brdo section and the Montclus (Morales et al., 2013), Hárskút (Lodowski et al., 2022) and Barlya (Grabowski et al., 2016) sections. Abbreviations: K.—Kimmeridgian; V.—Valanginian; L.—lower; U—Upper; B.—Boneti; C.—Colomi; Cad.—Cadischiana; Ch—Chitinoidella (Dobeni–Boneti); Crass.—Crassicollaria; Dar.—Darderi; Fer.—Ferasini; M.—Malmica; Mu.—Murgeanui; O—Otopeta; P.—Pertransiens; Pu.—Pulla; S—Semiradiata; Tith.—Tithonica; 1—Simplex; 2—Murgeanui; 3—ACME Parvula; 4—Moluccana; 5—Borzai; 6—Praetintinnopsella.

Tithonian age appears disputable due to regional correlations. Accordingly, Reháková and Rožič (2019) documented a single slump horizon from the lower Berriasian (Alpina/Ferasini subzonal boundary) of the Rudnica section (Figure 4b), which most likely provides the record of a distal, drowned part of the Dinaric Carbonate

Platform (Figure 1). In this context, it is noteworthy that sedimentary slumps and breccia horizons proved to be helpful in the correlation of Jurassic and Cretaceous sedimentary sequences of the Vocontian Basin (Courjault et al., 2011; Ferry, 2017). Besides, the interval directly below the slump in Petrovo Brdo is characterized by the occurrence of cherts (13–15 m), which may correspond to the lowermost Berriasian (Alpina Subzone) chert lenses in Rudnica (Reháková & Rožič, 2019). Based on the above considerations, it is proposed to place the J/K boundary between 13 and 20.8 m of the section.

Despite the fact that few specimens of *Calpionella alpina* were observed near the top of the section (sample PB39.5), some observations allow assignment of the interval between meters 26 and 40.6 to the upper Berriasian. That being said, clastic input is markedly increased above 26 m of the section (Figures 6 and 7). This correlates with an increase in magnetic susceptibility within the upper Berriasian Calpionellopsis Zone of the Rudnica section (Figure 4). The increase of clastic supply within the upper Berriasian beds is a supraregional Western Tethyan phenomenon, as observed in the Transdanubian Range (Lodowski et al., 2022), Balkan area (Grabowski et al., 2016; Grabowski, Stoykova, et al., 2021; Grabowski, Chmielewski, et al., 2021), Fatric succession of the Tatra Mountains (Grabowski & Pszczółkowski, 2006; Grabowski et al., 2013), as well as Northern Calcareous Alps (Krische et al., 2018) (see Figure 10a). Besides, a local peak in $\delta^{13}C$ around meter 30 of the section (Figure 5) may be correlated with a similar feature that marks the lower/upper Berriasian boundary interval (M16r/M16n magnetozones, lower part of Calpionellopsis calpionellid Zone) in other western Tethyan sections: Berrias and Montclus (Vocontian Basin; Emmanuel & Renard, 1993; Morales et al., 2013), Barlya (Western Balkan; Grabowski, Stoykova, et al., 2021) and Hárskút (Transdanubian Range; Lodowski et al., 2022) (Figure 10b). Noteworthy, this phenomenon might be equivalent to the "Middle Berriasian event" of Cramer and Jarvis (2020). Consequently, the presence of *Calpionella alpina* in the uppermost part of the section cannot be used as evidence for an early Berriasian age of the interval, especially when it is known that this taxon may occur as high as in the middle part of the upper Berriasian (Grabowski & Pszczółkowski, 2006; Grabowski et al., 2016).

5.2. Paleoenvironmental Interpretation

5.2.1. Detrital Elements

Potassium-based paleoclimate proxies (Al/K, Ti/K) are characterized by relatively low values at the Tithonian–Berriasian transition (cf. 5–20 m), which increase above and toward the top of the section (Figure 8). If adopt the mechanism of climate related leaching of potassium, such a record suggests relatively humid paleoclimate conditions during the early Tithonian, arid conditions during the late Tithonian–earliest Berriasian, and the humidification during the early/late Berriasian transition.

Grain size proxies (Zr/Al, Ti/Al) document a fine detrital fraction within the upper Tithonian–lowermost Berriasian (ca. 5–20 m), and a coarser fraction in both the lower Tithonian and the higher part of the Berriasian (Figure 8). Finer grain sizes are considered as reflecting rather low transportation energy (= ineffective uptake of heavier minerals) during the arid phase of climate. This kind of density fractionation might have been driven either by lowered wind energy (which supposedly was associated with climate cooling and aridization; see Lodowski, Szives, et al., 2024) and/or low riverine flux (due to lowered inland precipitation). Although rather remote (relative to continental masses), the paleogeographic setting of the Slovenian Basin would have favored the eolian transport although input via riverine plumes cannot be excluded.

However, there is a substantial difference in the records of Zr/Al and Ti/Al between the Slovenian Basin and the Bakony Basin (Transdanubian Range). In the Petrovo Brdo, they reach their minimal values around the Tithonian–Berriasian boundary (meters 10–15), whereas the corresponding interval in the Bakony Basin sections is characterized by elevated Zr/Al and lowered Ti/Al ratios (see Figure 6 and supplementary materials in Lodowski, Szives, et al., 2024). This apparent contradiction can be explained by the different paleogeographic settings of the two basins. The Bakony Basin not only extended toward the axial parts of the Alpine Atlantic but was also separated from the Neotethyan Collision Belt and the Neotethys Ocean by the Gerecse Basin. Such a remote paleogeographic position is also suggested by very limited clastic admixture (even below 0.1% Al; see Figures 1 and 5 in Lodowski et al., op cit.). Consequently, the supply and composition of the terrigenous fraction may have been affected by changes in the efficiency of eolian transportation. During the arid climatic phase, clastic influx was restricted by low weathering rates, yet the eolian fraction may potentially spread over large distances due to low precipitation. Under such conditions, elemental ratios in remote areas, such as the Bakony Basin, may have been affected by material coming from far source areas, and consequently relatively enriched in Zr. In contrast, the Slovenian Basin

extended eastwards and would have received an unrestricted supply of clastic material from the area of the Neotethyan Collision Belt (Figure 1). Therefore, grain size proxies may better record fractionation processes in their source areas, regardless of whether they were eolian or took place on marine shelfs or slopes.

It can also be noted that increasing concentrations of lithogenic elements in the Petrovo Brdo section (from ca. 25 m) might have resulted from the cumulative effects of early/late Berriasian climatic change (humidification; i.e., Deconinck, 1993; Morales et al., 2013) and reactivation and uplift of the Neotethyan Collision Belt (Fodor et al., 2013; Gawlick et al., 2009; Lodowski et al., 2022; Lodowski, Szives, et al., 2024), when land exposure and erosion led to intensified terrigenous flux to neighboring sedimentary basins in the late Berriasian.

5.2.2. Paleoredox Proxies Versus Nutrient-Type Trace Metals

The main trends observed in paleoredox proxies (authigenic U, U/Th) appear to reflect nutrient-type trace elements (Figure 9; Supporting Information 3 in https://doi.org/10.5281/zenodo.12542820). Both authigenic U and U/Th document a gradual increase up to meter 23 of the section. The general record provided by "excess" portions of Ba, Cu and Zn is similar; however, they increase sharply at the Tolmin/Biancone formational boundary (meter 5) and remain steadily elevated above, up to meter 25 (interval II on Figure 9). In turn, enrichment factors of "productive" elements increase near meter 5 but begin to decrease thereafter (Supporting Information 3 in https://doi.org/10.5281/zenodo.12542820). Finally, elevated TOC/Al at the base of the Biancone Limestone (5–15 m) not only falls within elevated "excess" Ba, Cu and Zn but also correlates with their maximum EF's and slightly increasing U-based indices (compare Figure 9 with Supporting Information 3.7–3.8 in https://doi.org/10.5281/zenodo.12542820). Consequently, both paleoredox and productivity-related proxies manifest positive shifts within the upper Tithonian–lowermost Berriasian beds.

The interval between meters 23 and 27 records decreasing values of U-based proxies. Similarly, "excess" concentrations of Ba, Cu and Zn decrease above meter 25, while their EFs manifest local lows. Ultimately, the topmost 12.5 m of the section are characterized by elevated TOC (and low TOC/Al), which corresponds to elevated clastic supply as well as slightly increasing paleoredox proxies and micronutrient content (Figures 7 and 9; Supporting Information 3 in https://doi.org/10.5281/zenodo.12542820).

Accordingly, it seems that both U-fixation in sediments and nutrient burial was most likely controlled by a common mechanism, as proposed recently by Lodowski and Grabowski (2023) and Lodowski, Szives, et al. (2024). It relies on the fact that relative oxygen depletion at the seafloor indicates stratification, while restricted mixing of the water column allows a greater amount of micronutrients to be trapped at the seafloor, causing their enrichment within sediment and lowered surface productivity. The two intervals with elevated TOC (upper Tithonian–lowermost Berriasian and lower/upper Berriasian transition; Figure 7) additionally confirm that some (limited) changes in oxygenation might have occurred, whereas increased burial of "authigenic" organic matter (TOC/Al) at the Tithonian/Berriasian boundary interval (Figure 9) evidences perturbations in water mixing and the nutrient uptake.

Furthermore, the above model not only helps to understand the co-variations of observed paleoredox and trace metal indices of the Petrovo Brdo section but also can explain the low EFs and biological fluxes of nutrient-type elements within the radiolarite Tolmin Fm. (0–5 m). Radiolarites are typically considered to be reflective of a productive ocean, when extraordinary large amounts of nutrients were delivered to the photic zone either from lands (i.e., via river plumes; see Baumgartner, 2013) and/or by upwelling currents, which steadily uptake (recycle) them within the water column (the so-called "nutrient shuttle"). In this context, whenever the water mixing processes decrease in intensity, a higher amount of nutrients sink and become trapped in sediment. Consequently, even though radiolarites represent a productive state, this does not directly translate into sediment geochemistry. In this case, the productive sea-surface is manifested by relatively low concentrations of nutrient-type elements (their EFs and/or "biogenic" concentrations)—and vice versa in case of carbonates ("oligotrophic" ocean).

6. Discussion

6.1. Correlation With the Transdanubian Range and Other Areas—Paleoenvironmental Implications

Paleogeographic proximity between the Slovenian Basin and the Bakony Basin (Figure 1) suggests that their sedimentary successions provide a similar record of past trends and events. Consequently, this study compares

paleoenvironmental signals obtained in the Petrovo Brdo section with the data collected in the Hárskút and Lókút successions of the Transdanubian Range (Lodowski, Szives, et al., 2024; see also Grabowski et al., 2017).

6.1.1. Paleoclimate of the Tithonian–Berriasian

Regardless of the potential for different reliability of detrital paleoclimate proxies (Figure 8; see also Supporting Information 3 and 4 in https://doi.org/10.5281/zenodo.12542820), the section can be divided into three intervals of discrete paleoclimate significance. Interval I (radiolarites of the Tolmin Fm.) is characterized by: (a) relatively high terrigenous and silica content and low carbonate content; as well as (b) relative depletion in K and enrichment in Ti (high Al/K, Ti/K and Ti/Al), most likely also in Zr (elevated Zr/Al and Zr/Rb). The succeeding interval II (lower part of the Biancone Limestone Fm.) documents: (a) low terrigenous and high carbonate content and (b) relative enrichment in K and depletion in Ti (low Al/K, Ti/K and Ti/Al). Finally, interval III (upper part of the Biancone Limestone Fm.) is quite similar to the interval I, and is characterized by: (a) increasing and elevated terrigenous influx; as well as (b) elevated values of Al/K, Ti/K, Ti/Al, Zr/Al, and Zr/Rb.

The geochemistry of intervals I and III reflect a humid paleoclimate, whereas interval II points to arid conditions. This record is coherent not only with the data from the Transdanubian Range (Figure 11) but also the Vocontian Basin (Deconinck, 1993; Morales et al., 2013) and the European Platform (e.g., Abbink et al., 2001; Grabowski, Chmielewski, et al., 2021; Schneider et al., 2018; Schnyder et al., 2006). In the Transdanubian Range, the onset of aridification can be traced within the lowermost upper Tithonian, in the middle part of magnetozone M20n (base of the Crassicollaria calpionellid Zone; Lodowski, Szives, et al., 2024), which corresponds well with the inferred age of the base of the Biancone Limestone Fm., and the boundary between paleoenvironmental intervals I and II (see Section 5.1). Recent dating of the latest Jurassic/earliest Cretaceous aridization event on the European Platform points to Panderi/Virgatus boreal ammonite zonal boundary (middle Volgian; Błażejowski et al., 2023). This, in turn, can be correlated with the base of the Portlandian (Fittoni/Albani Sub-Boreal ammonite zonal boundary) as well as with the Chitinoidella boneti calpionellid Subzone (lower part of M20n). Based on the above, the onset of climate aridization in the Tethyan and Sub-Boreal domains would be almost coeval.

In the Transdanubian Range, the subsequent humidification event falls within the boundary interval between the lower and upper Berriasian (magnetozoneM16r, base of Calpionellopsis calpionellid Zone; Lodowski, Szives, et al., 2024). The dating must be interpreted as approximate due to the condensed nature of the Hárskút succession (Lodowski et al., 2022). In the Vocontian Basin (Berrias and Montclus sections), the first shift toward more humid conditions can be estimated as occurring during the mid-M17r magnetozone (Calpionella elliptica Subzone, uppermost lower Berriasian), as inferred from clay mineral data of Deconinck (1993), and recent stratigraphic refinement of the Berrias section made by Wimbledon et al. (2024). Accordingly, the base of the interval III in the Petrovo Brdo section (ca. 25 m) seems to fall within the upper part of the lower Berriasian (Figures 8 and 10), and thus is coeval with the onset of humidification in the Vocontian Basin.

6.1.2. Oceanographic Conditions During the Jurassic–Cretaceous Transition

This study emphasizes the importance of (climate induced) changes in water circulation for surface productivity and resultant sedimentary patterns. Although the latest Jurassic was deprived of mass volcanism, what likely resulted in lowered pCO_2 and deepening of CCD (see , i.e., Weissert & Erba, 2004; Weissert & Mohr, 1996), this long-term trend cannot be considered as the main (or only) factor controlling carbonate productivity in the Slovenian Basin. At first, the CCD-based model of carbonate/radiolarite distribution fails in many cases (i.e., radiolarians are rare and often calcified in condensed pelagic limestones) and lately, attention has been drawn to the issue of marine fertility (i.e., Baumgartner, 2013). Furthermore, since the Tithonian was a time of tectonic quietness, either the depth of the CCD and/or the chemistry of the Slovenian Basin could not have been affected by any substantial changes in marine currents. Finally, in modern environments, biocalcification is stimulated by low seawater temperatures and a corresponding mechanism was proposed to explain the phenomenon of nannofossil calcification events (NCE'S; Casellato, 2009).

Similar trends in geochemical proxies of seafloor oxidation and deposition (burial) of nutrient-type trace elements occur in both the Slovenian Basin and the Transdanubian Range (Bakony Basin). They are characterized by the trace metal enrichment within the Tithonian/Berriasian transition interval (Figure 11a), which is also associated with elevated values of paleoredox indices (Figure 11b). On this basis, the paleoenvironmental model which Lodowski, Szives, et al. (2024) applied to the area of the Transdanubian Range can be extended to the Slovenian

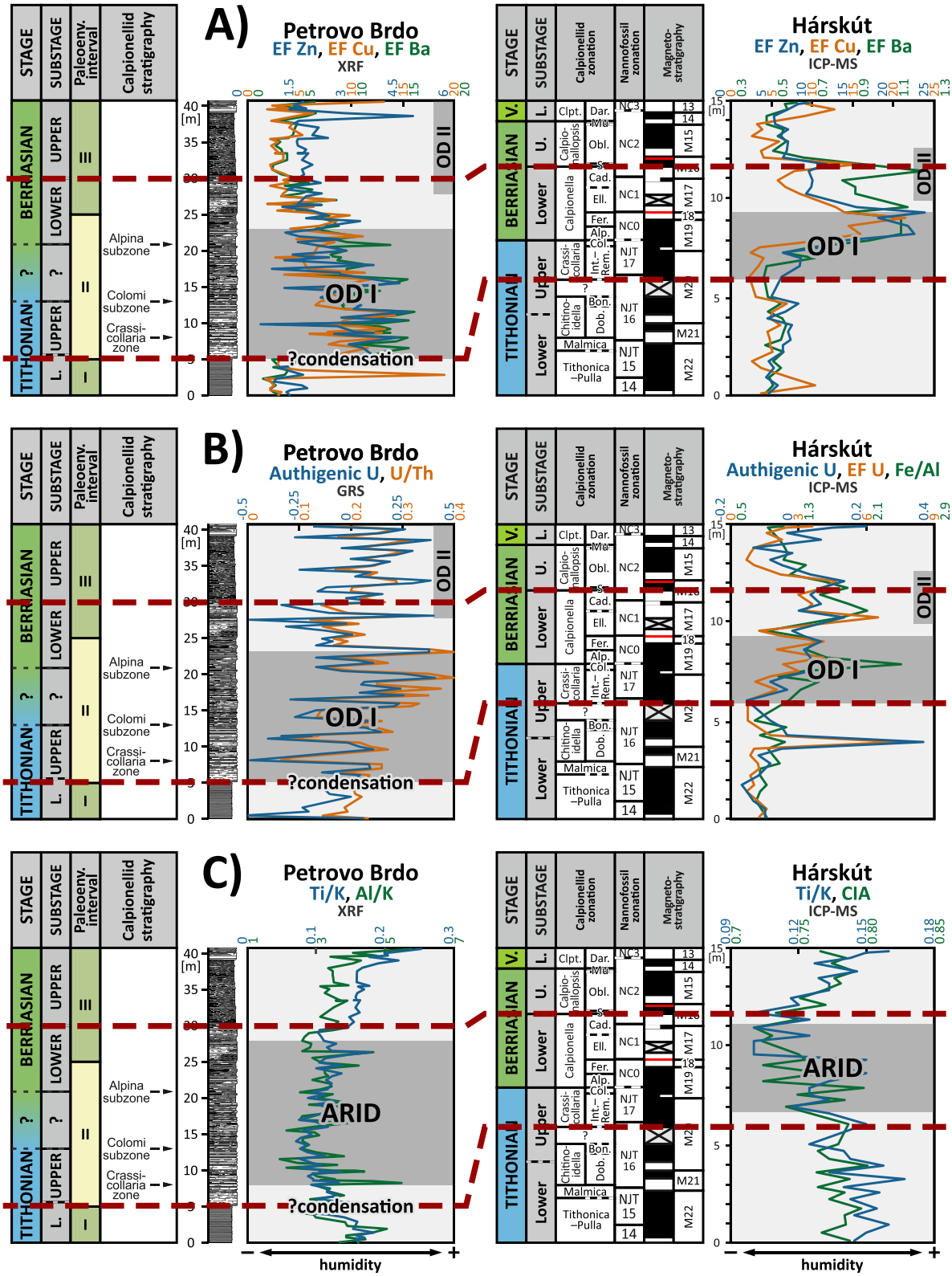

Figure 11. Selected proxies for micronutirent concentrations (a), seafloor oxidation (b) and paleoclimate (c) in the Petrovo Brdo and Transdanubian Range sections. Abbreviations: V.—Valanginian; L.—Lower; U—Upper; Alp.—Alpina; Bon.—Boneti; Cad.—Cadischiana; Clpt.—Calpionellites; Col.—Colomi; Dar.—Darderi; Dob.—Dobeni; Ell.—Elliptica; Int.—Intermedia; Mu.—Murgeanui; Obl.—Oblonga; Rem.—Remanei; S.—Simplex.

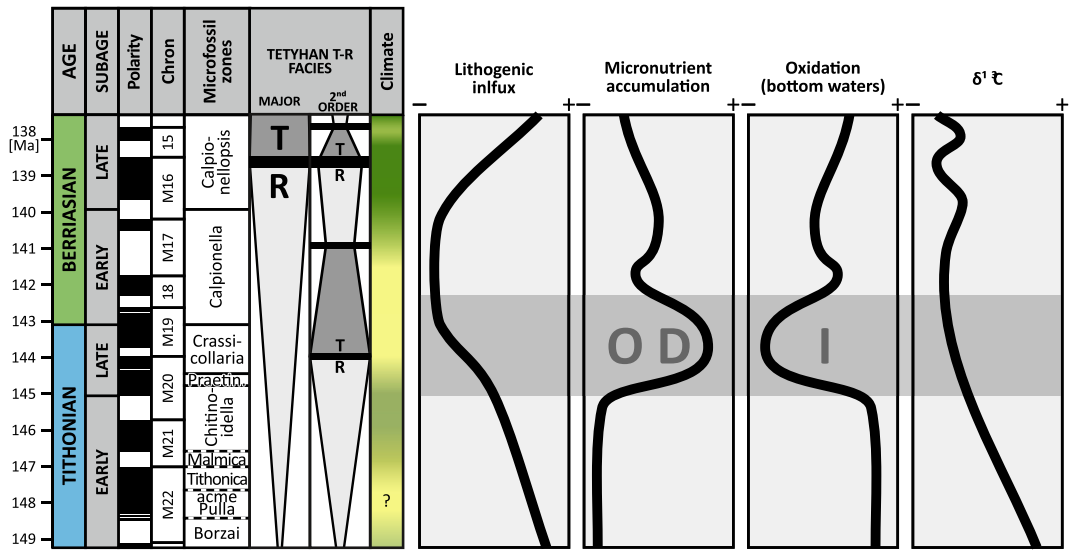

Figure 12. Generalized paleoenvironmental trends during the Tithonian–Berriasian. Transgressive-regressive (T-R) cycles after Hardenbol et al. (1998); paleoclimate interpretation after Lodowski and Grabowski (2023) and Lodowski et al. (2024); lithogenic influx, surface productivity, seafloor oxidation and $\delta^{13}C$ trends as presented in this study and in Lodowski et al. (op cit.).

Basin. Accordingly, the relatively cool and arid climate of the late Tithonian–early Berriasian is thought to have weakened atmospheric circulation and wind-induced water currents (i.e., monsoonal upwellings; see Lodowski, Szives, et al., 2024). This, in turn, limited water mixing and promoted stratification, resulting in seafloor hypoxia. Nutrient-shuttle mechanisms were also disrupted, as manifested by their increased burial (paleoenvironmental interval II on Figure 9; OD I in Lodowski, Szives, et al., 2024; see also Figure 12). Noteworthy, this model differs from the classical approach, where increased amounts of Zn, Ba, or Cu in sediments are interpreted as productivity proxies (Tribovillard et al., 2006), and conforms rather to Calvert and Pedersen (2007), who mention them as related to low-oxygen sedimentation (not denying their importance as micronutrients).

Early/late Berriasian environmental perturbations documented in the Transdanubian Range (OD II "event" in Lodowski, Szives, et al., 2024) can also be recognized within the Petrovo Brdo section. Slightly elevated trace metal enrichment (at the topmost part of the section) and U indices (above meter 30) (Figures 11a and 11b) along with increasing lithogenic influx and humidity indicators (Figure 11c) within the upper Berriasian seem to correlate with the records from the Transdanubian Range (see Figures 7 and 8 in Lodowski et al., op cit.). Consequently, tectonic reactivation and uplift in the Neotethyan Collision Belt (NCB) may have also affected the Slovenian Basin. Similarly, like the Bakony Basin, it could have been cut off from oceanic and atmospheric circulation patterns of the western Neotethys, which limited the oceanographic effect (i.e., induction of monsoonal upwellings) of generally humid late Berriasian. However, it must be taken into account that correlations in the upper Berriasian are not as precise due to the lack of biostratigraphic proxies in the Petrovo Brdo section and condensation/slow sedimentation rates in Hárskút.

It is also noteworthy that some pioneer geochemical data from the Tithonian/Berriasian boundary interval of the Neuquén Basin (Argentina) document a very similar record of paleoenvironmental proxies, both in terms of seafloor oxygenation and enrichment in nutrient-type trace metals (compare Figure 13 in Capelli et al., 2021 with Figure 11 herein). Recently, Capelli et al. (2024) documented kaolinite from the lower/upper Berriasian boundary interval of the Neuquén Basin (Elliptica/Simplex calpionellid zones), what corresponds with paleoclimate record know from European sections. Furthermore, middle Volgian enrichment in trace metals in NE Greenland (Hovikoski et al., 2023) and Arctic Canada (Galloway et al., 2024) were interpreted as primarily related to local/regional tectonics. However, this event can be approximated as not earlier than M20n and not later than M17r (late Tithonian–earliest Berriasian; see Grabowski, Chmielewski, et al., 2021); therefore, some other effects should also be taken into consideration. Such correlation not only suggests that the latest Jurassic/earliest Cretaceous climate changes might have had a global scope but also that paleoenvironmental conditions (atmospheric

circulation, water mixing, seafloor oxidation, seawater nutrition) might have been largely controlled by similar (if not the same) mechanisms, that is, climate cooling/warming and related decreasing/increasing (respectively) intensity of up-/downwelling currents. Nonetheless, this hypothesis requires further testing in various regions of the world.

6.1.3. Eustatic Sea-Level Changes and Tectonism—Neglectable Effects?

This study does not consider eustasy amongst factors which could potentially affect the latest Jurassic/earliest Cretaceous clastic supply and, indirectly, the sedimentary geochemical record. The Tithonian–early Berriasian was marked by general regression, which in most cases (except some specific near-shore settings) should result in increasing clastic input (due to lowering of erosional base, e.g., Ellwood et al., 2000), the opposite to what is observed. Furthermore, Ray et al. (2019) estimated Berriasian sea-level changes as below 10 m, likely to little to affect such remote pelagic areas such as the Slovenian and Bakony basins. Interestingly, the 1st order regressive (Tithonian–early Berriasian) and the subsequent transgressive trends (Figure 12; Haq, 2014, 2018; Hardenbol et al., 1998) correlate with general climate tendencies: aridization and humidification, respectively. Consequently, these sea-level variations might be considered as predominantly glacio-esutatic (Price, 1999; van der Meer et al., 2022).

In the Alpine Atlantic region, the Tithonian–early Berriasian period was a time of tectonic quietness. Although there are some evidences for limited tectonic activity during the Tithonian (Lodowski & Grabowski, 2023), no major tectonic event happened until the early late Berriasian (early M16n chron), when the Neotethyan Collision Belt became (re)activated (for more see Lodowski, Szives, et al., 2024 and references therein). Therefore, the late Tithonian–earliest Berriasian oceanographic perturbations (OD I event) could not have been driven by tectonically forced changes in marine circulation, while the general fall in the amount of lithic elements can be considered as an echo of tectonic stability, with extensive peneplains and eroded islands.

6.2. Characteristics of the Latest Jurassic–Earliest Cretaceous Marine Hypoxia

Paleoenvironmental conditions during the Jurassic/Cretaceous transition substantially differed from those characterizing oceanic anoxic events (OAE's). In particular, the J/K transition was the coolest interval of the entire Mesozoic era (i.e., Scotese et al., 2021; van der Meer et al., 2022), while OAE's were typically related to enhanced volcanism and climate warming (Gradstein et al., 2020; Meyer & Kump, 2008). Furthermore, OAE's were associated with extraordinary (anoxic to euxinic) conditions, which commonly resulted in faunal crises, deposition of black shales with elevated TOC, and enrichment in certain trace elements (i.e., Jenkyns, 2010); due to that, such events are relatively well expressed even in outcrop scale. In turn, the Tithonian–Berriasian sedimentary successions account for a rather undifferentiated lithologic appearance, they are devoid of any significant faunal turnover (Wimbledon et al., 2020), and lack any characteristic isotopic excursion (Price et al., 2016). With that respect, the Tithonian–Berriasian oceanographic perturbations (OD I herein) should not be identified as or compared to OAE-type events which started during the Aptian period when greenhouse/hothouse conditions were established (i.e., Ruffel et al., 2002).

In both the Slovenian Basin and the Transdanubian Range (see Lodowski, Szives, et al., 2024), paleoredox proxies point to decreased availability of oxygen (hypoxia) under a generally oxic regime; this should not be confused with dysoxia and/or anoxia, which is characterized by the lack or biologically insufficient oxygen. Unlike OAE periods, oceanographic conditions during the latest Jurassic–earliest Cretaceous were primarily related to climate-induced (cooling) changes in atmospheric circulation. Sedimentary and biotic responses to these perturbations were limited, as evidenced by long-lasting discussions on the position of the J/K boundary (Énay, 2020; Wimbledon et al., 2020). However, even if of limited scope, stratification and the slowdown in marine circulation resulted in increased burial rates of micronutrients, regardless of their low content (Figure 11a). That being said, from an oceanographic point of view, the OD I event should be regarded as reflecting some minor perturbations in the marine ecosystem, yet characteristic for the Tithonian/Berriasian boundary interval, at least for the western Tethyan successions.

7. Conclusions

1. An integrated stratigraphy approach enabled a complex stratigraphic calibration of the Petrovo Brdo section. A limited biostratigraphic framework provided by calcareous dinocysts and calpionellids (Figure 2) was

integrated with magnetic susceptibility correlations (Figure 4b), $\delta^{13}C$ stratigraphy (Figure 10b), and systematic evaluation and correlation of different paleoenvironmental signals documented in the Slovenian Basin and the Transdanubian Range sections (Figure 11; Lodowski, Szives, et al., 2024). On this basis, the base of the Biancone Limestone Fm. in the Petrovo Brdo section falls in the lower part of the upper Tithonian (magnetozone M20n). The Tithonian/Berriasian boundary (base Alpina Subzone) cannot be precisely located but is most likely situated within the interval of lowered lithogenic input and minimum of $\delta^{13}C$ values. The lower/upper Berriasian boundary was placed within the interval characterized by increasing lithogenic influx and a distinct peak in $\delta^{13}C$, correlatable with similar signals known from other western Tethyan sections (Figure 10b).

2. The Petrovo Brdo section is characterized by three distinct paleoenvironmental phases. The lower Tithonian of the Tolmin Fm. (interval I, 0–5 m) was deposited under a humid paleoclimate in a regime of well-mixed water column and oxic bottom water conditions. The Tithonian/Berriasian transition (interval II, 5–27.5 m, lower part of the Biancone Limetsone Fm.) was characterized by a relatively arid climate and a stratified water column. Finally, during the late Berriasian (interval III, above meter 27.5, upper part of the Biancone Limestone Fm.), a phase of climate humidification with elevated clastic supply occurred (Figures 7–9); however, the water column was only limitedly mixed. The aridization event corresponds to a similar phenomenon documented in the Transdanubian Range sections by Lodowski, Szives, et al. (2024; see OD I therein), what confirms the importance of the late Tithonian–early Berriasian climate change and its effect on marine circulation in the Alpine Atlantic. Important and likely supraregional in scale was also the early/late Berriasian tectonic reactivation in the Neotethyan Collision Belt. Not only did it result in a significant increase in clastic input, but it might also cut both the Slovenian and the Bakony basins off from the Neotethys Ocean, thus limiting the effect of climate humidification (=increasing wind energy) on water mixing processes (see also Lodowski, Szives, et al., 2024).
3. A very sharp contrast observed in enrichment factors of nutrient-type elements (Zn, Cu, Ba; Figure 9) between the Tolmin Fm. and the base of Biancone Limestone (5 m of the section) confirms the oceanographic model of Lodowski, Szives, et al. (2024). The lower Tithonian radiolarites correspond to a 'productive ocean' (sea surface), when nutrients are constantly recycled within the upper ocean due to strong winds (i.e., monsoonal upwellings; see also De Wever et al., 2014). In turn, the early/late Tithonian climate change (aridization) was associated with decreasing atmospheric energy and less efficient induction of water mixing processes. This reduced the availability of oxygen at the seafloor and allowed micronutrients to sink and become incorporated in sediments (Figure 9). Consequently, this study unambiguously proves the occurrence of an inversed relationship between the relative content of nutrient-type trace metals in sediments and surface productivity.
4. Major palaeoenvironmental turnovers in the Slovenian basin and the Transdanubian Range: the mid-Tithonian aridization and the mid-Berriasian humidification correlate with similar climatic events documented in the Vocontian Basin and Sub-boreal domain (Polish Basin, North Sea, southern England and Northern France). This suggests that the common paleoclimatic signals can serve as helpful chronostratigraphic correlation tools, even when considering different paleobiogeographic domains.

Acknowledgments
We would like to send our warmest thanks to Ottilia Szives, David Gercar and István Főzy for their help during the field works and discussions on collected material. The authors would also like to thank the journal reviewers (Jennifer Galloway, Thomas Algeo and one anonymous reviewer) and the editorial team for their constructive comments and efforts to improve the current paper. These investigations were financially supported by the National Science Center, Poland (project no.: 2016/21/B/ST/10/02941; leader: J. Grabowski, PGI-NRI, Warsaw) and Slovak grant agencies APVV (Agentúra na Podporu Výskumu a Vývoja) and VEGA (Vedecká Grantová Agentúra MŠVVaŠ SR a SAV); projects no: APVV 20-0079 and VEGA 2/0012/24 (leader: J. Soták, Earth Science Institute of the Slovak Academy of Sciences).

Data Availability Statement

The data produced during this study have been uploaded to the Zenodo online re-pository (Lodowski, Grabowski, et al., 2024; https://doi.org/10.5281/zenodo.12542820).

References

Abbink, J., Targona, J., Brinkhuis, H., & Visscher, H. (2001). Late Jurassic to earliest Cretaceous palaeoclimatic evolution of the southern North Sea. *Global and Planetary Change*, *30*(3–4), 231–256. https://doi.org/10.1016/S0921-8181(01)00101-1

Algeo, T. J., & Liu, J. (2020). A re-assessment of elemental proxies for paleoredox analysis. *Chemical Geology*, *540*, 119549. https://doi.org/10.1016/j.chemgeo.2020.119549

Alley, N. F., Hore, S. B., & Frakes, L. A. (2020). Glaciations at high-latitude of Southern Australia during the Early Cretaceous. *Australian Journal of Earth Sciences*, *67*(8), 1045–1095. https://doi.org/10.1080/08120099.2019.1590457

Arnaud, F., Révillon, S., Debret, M., Revel, M., Chapron, E., Jacob, J., et al. (2012). Lake Bourget regional erosion patterns reconstruction reveals Holocene NW European Alps soil evolution and paleohydrology. *Quarternary Science Reviews*, *51*, 81–92. https://doi.org/10.1016/j.quascirev.2012.07.025

Baumgartner, P. O. (2013). Mesozoic radiolarites – Accumulation as a function of sea surface fertility on Tethyan margins and in ocean basins. *Sedimentology*, *60*(1), 292–318. https://doi.org/10.1111/sed.12022

Behar, F., Beaumont, V., & de Penteado, B. (2001). Rock-Eval 6 Technology: Performance and developments. *Oil and Gas Science and Technology*, *56*(2), 111–134. https://doi.org/10.2516/ogst:2001013

Błażejowski, B., Pszczółkowski, A., Grabowski, J., Wierzbowski, H., Deconinck, J.-F., Olempska, E., et al. (2023). Integrated stratigraphy and clay mineralogy of the Owadów-Brzezinki section (lower-upper Tithonian transition, Central Poland): Implications for correlations between the Boreal and the Tethyan domains and palaeoclimate. *Journal of the Geological Society*, *180*(2). https://doi.org/10.1144/jgs2022-073

Bornemann, A., Aschwer, U., & Mutterlose, J. (2003). The impact of calcareous nannofossils on the pelagic carbonate accumulation across the Jurassic–Cretaceous boundary. *Palaeogeography, Palaeoclimatology, Palaeoecology*, *199*(3–4), 187–228. https://doi.org/10.1016/S0031-0182(03)00507-8

Bralower, T. J., Monechi, S., & Thierstein, H. R. (1989). Calcareous nannofossil zonation of the Jurassic-Cretaceous boundary interval and correlation with the geomagnetic polarity timescale. *Marine Micropaleontology*, *11*(1–3), 153–235. https://doi.org/10.1016/0377-8398(89)90035-2

Buser, S. (1989). Development of the Dinaric and Julian carbonate platforms and the intermediate Slovenian basin (NW-Yugoslavia). In G. B. Carulli, F. Cucchi, & C. P. Radrizzani (Eds.), *Evolution of the Karstic carbonate platform: Relation with other periadriatic carbonate platforms* (Vol. 40, pp. 313–320). Memoire della Società Geologica Italiana.

Buser, S. (1996). Geology of the western Slovenia and its paleogeographic evolution. In K. Drobne, Š. Goričan, & B. Kotnik (Eds.), *The role of impact processes in the geological and biological evolution of planet Earth*, *International Workshop* (pp. 111–123). ZRC SAZU.

Calvert, S. E., & Pedersen, T. F. (2007). Elemental proxies for palaeoclimatic and palaeoceanographic variability in marine sediments: Interpretation and application. *Developments in Marine Geology*, *1*, 567–644. https://doi.org/10.1016/S1572-5480(07)01019-6

Capelli, I. A., Scasso, R. A., Spangenberg, J. E., Kietzmann, D. A., Cravero, F., Duperron, M., & Adatte, T. (2021). Mineralogy and geochemistry of deeply-buried marine sediments of the Vaca Muerta-Quintuco system in the Neuquén Basin (Chacay Melehue section), Argentina: Paleoclimatic and paleoenvironmental implications for the global Tithonian-Valanginian reconstructions. *Journal of South American Earth Sciences*, *107*, 103103. https://doi.org/10.1016/j.jsames.2020.103103

Capelli, I. A., Scasso, R. A., Spangenberg, J. E., Kietzmann, D. A., Prámparo, M., & Adatte, T. (2024). Paleoenvironmental reconstruction of the Berriasian organic-rich interval of the Vaca Muerta Formation (Neuquén Basin, Argentina): Insights for the characterization of unconventional hydrocarbon shale reservoirs. *Marine and Petroleum Geology*, *163*, 106760. https://doi.org/10.1016/j.marpetgeo.2024.106760

Casellato, C. E. (2009). *Causes and Consequences of calcareous Nannoplankton Evolution in the Late Jurassic: Implications for Biogeochronology, Biocalcification and Ocean Chemistry* Ph.D. Thesis (p. 122). Universita degli Studi di Milano.

Casellato, C. E., & Erba, E. (2021). Reliability of calcareous nannofossil events in the Tithonian–early Berriasian time interval: Implications for a revised high resolution zonation. *Cretaceous Research*, *117*, 104611. https://doi.org/10.1016/j.cretres.2020.104611

Cavalheiro, L., Wagner, T., Steinig, S., Bottini, C., Dummann, W., Esebegue, O., et al. (2021). Impact of global cooling on Early Cretaceous high pCO_2 world during the Weissert Event. *Nature Communications*, *12*(1), 5411. https://doi.org/10.1038/s41467-021-25706-0

Cope, J. C. W. (2008). Drawing the line: The history of the Jurassic—Cretaceous boundary. *Proceedings of the Geologists' Association*, *119*(1), 105–117. https://doi.org/10.1016/S0016-7878(08)80262-3

Courjault, T., Grosheny, D., Ferry, S., & Sausse, J. (2011). Detailed anatomy of a deep-water carbonate breccia lobe (Upper Jurassic, French subalpine basin). *Sedimentary Geology*, *238*(1–2), 156–171. https://doi.org/10.1016/j.sedgeo.2011.04.010

Cramer, B. D., & Jarvis, I. (2020). Carbon isotope stratigraphy. In F. M. Gradstein, J. G. Ogg, M. D. Schmitz, & G. M. Ogg (Eds.), *Geologic time scale 2020* (pp. 309–344). Elsevier. https://doi.org/10.1016/B978-0-12-824360-2.00011-5

Deconinck, J. F. (1993). Clay mineralogy of the Late Tithonian—Berriasian deep-sea carbonates of the Vocontian Trough (SE France): Relationships with sequence stratigraphy. *Bulletin des Centres de Recherches Exploration-Production Elf-Aquitaine*, *17*, 223–234.

Demšar, M. (2016). *Geological map of the Selca valley 1:25.000*. Geological Survey of Slovenia.

De Wever, P., O'Dogherty, L., & Goričan, Š. (2014). Monsoon as a cause of radiolarite in the Tethyan realm. *Comptes Rendus Geoscience*, *346*(11–12), 287–297. https://doi.org/10.1016/j.crte.2014.10.001

Ellwood, B. B., Crick, R. E., Hassani, A. E., Benoist, S. L., & Young, R. H. (2000). Magnetosusceptibility event and cyclostratigraphy method applied to marine rocks: Detrital input versus carbonate productivity. *Geology*, *28*(12), 1135–1138. https://doi.org/10.1130/0091-7613(2000)28<1135:MEACMA>2.0.CO;2

Emmanuel, L., & Renard, M. (1993). Carbonate geochemistry (Mn, $\delta^{13}C$, $\delta^{18}O$) of the late Tithonian–Berriasian pelagic limestones of the Vocontian trough (SE France). *Bulletin des Centres de Recherches Exploration-Production Elf-Aquitaine*, *17*, 205–221.

Énay, R. (2020). The Jurassic/Cretaceous System Boundary is at an impasse. Why not go back to Oppel's 1865 original and historic definition of the Tithonian? *Cretaceous Research*, *106*, 104241. https://doi.org/10.1016/j.cretres.2019.104241

Espitalié, J., Deroo, G., & Marquis, F. (1985). La pyrolyse Rock-Eval et ses applications; première partie. *Revue de l'Institut Français du Petrole*, *40*(5), 563–579. https://doi.org/10.2516/ogst:1985035

Ferry, S. (2017). Summary on Mesozoic carbonate deposits of the Vocontian trough (subalpine Chains, SE France). In B. Granier (Ed.), *Some key Lower Cretaceous sites in Drôme (SE France)* (Vol. 2017, pp. 9–42). Carnets de Geologie.

Fodor, L., Sztanó, O., & Kövér, S. (2013). Mesozoic deformation of the northern Transdanubian Range (Gerecse and Vértes Hills). *Acta Mineralogica-Petrographica*, *31*, 1–52.

Föllmi, K. B. (2012). Early Cretaceous life, climate and anoxia. *Cretaceous Research*, *35*, 230–257. https://doi.org/10.1016/j.cretres.2011.12.005

Galloway, J., Hadlari, T., Dewing, K., Poulton, T., Grasby, S. E., Reinhardt, L., et al. (2024). The silent VOICE – Searching for geochemical markers to track the impact of the Late Jurassic rift tectonics. *Geochemistry, Geophysics, Geosystems*, *25*(10), e2024GC011490. https://doi.org/10.1029/2024GC011490

Gawlick, H.-J., Missoni, S., Schlagintweit, F., Suzuki, H., Frisch, W., Krystyn, L., & Lein, R. (2009). Jurassic tectonostratigraphy of the austroalpine domain. *Journal of Alpine Geology*, *50*, 1–152.

Goričan, Š., Kosir, A., Rožič, B., Smuc, A., Gale, L., Kukoc, D., et al. (2012). Mesozoic deep-water basins of the eastern Southern Alps (NW Slovenia). Field Trip Guide. 29th IAS Meeting of Sedimentology, Schladming, Austria. *Journal of Alpine Geology*, *54*, 101–143.

Goričan, Š., Pavšič, J., & Rožič, B. (2012). Bajocian to Tithonian age of radiolarian cherts in the Tolmin basin (NW Slovenia). *Bulletin de la Societe Geologique de France*, *183*(4), 369–382. https://doi.org/10.2113/gssgfbull.183.4.369

Goričan, Š., Žibret, L., Košir, A., Kukoč, D., & Horvat, A. (2018). Stratigraphic correlation and structural position of Lower Cretaceous flysch-type deposits in the eastern Southern Alps (NW Slovenia). *International Journal of Earth Sciences*, *107*(8), 2993. https://doi.org/10.1007/s00531-018-1636-4

Grabowski, J., Aguirre-Urreta, B., Deconinck, J.-F., Erba, E., Frau, C., Li, G., et al. (2022). Recent progress in defining the Tithonian/Berriasian and Jurassic/Cretaceous boundaries. In J. W. M. Jagt, E. Jagt-Yazykova, I. Walaszczyk, & A. Żylińska (Eds.), *11th Cretaceous Symposium, Warsaw, Poland 2022. Abstract Volume* (pp. 172–174). University of Warsaw.

Grabowski, J., Bakhmutov, V., Kdýr, Š., Krobicki, M., Pruner, P., Reháková, D., et al. (2019). Integrated stratigraphy and palaeoenvironmental interpretation of the Upper Kimmeridgian to Lower Berriasian pelagic sequences of the Velykyi Kamianets section (Pieniny Klippen Belt, Ukraine). *Palaeogeography, Palaeoclimatology, Palaeoecology*, *532*, 109216. https://doi.org/10.1016/j.palaeo.2019.05.038

Grabowski, J., Chmielewski, A., Ploch, I., Rogov, M., Smoleń, J., Wójcik-Tabol, P., et al. (2021). Palaeoclimatic changes and inter-regional correlations in the Jurassic/Cretaceous boundary interval of the polish basin: Portable XRF and magnetic susceptibility study. *Newsletters on Stratigraphy*, *54*(2), 123–158. https://doi.org/10.1127/nos/2020/0600

Grabowski, J., Haas, J., Stoykova, K., Wierzbowski, H., & Brański, P. (2017). Environmental change around the Jurassic/Cretaceous transition: New nannofossil, chemostratigraphic and stable isotope data from the Lókút section (Transdanubian Range, Hungary). *Sedimentary Geology*, *360*, 54–72. https://doi.org/10.1016/j.sedgeo.2017.08.004

Grabowski, J., Lakova, I., Petrova, S., Stoykova, K., Ivanova, D., Wójcik-Tabol, P., et al. (2016). Paleomagnetism and integrated stratigraphy of the Upper Berriasian hemipelagic succession in the Baryla section Western Balkan, Bulgaria: Implications for lithogenic input and paleoredox variations. *Palaeogeography, Palaeoclimatology, Palaeoecology*, *461*, 156–177. https://doi.org/10.1016/j.palaeo.2016.08.018

Grabowski, J., & Pszczółkowski, A. (2006). Magneto- and biostratigraphy of the Tithonian–Berriasian pelagic sediments in the Tatra Mountains (central Western Carpathians, Poland): Sedimentary and rock magnetic changes at the Jurassic/Cretaceous boundary. *Cretaceous Research*, *27*(3), 398–417. https://doi.org/10.1016/j.cretres.2005.07.007

Grabowski, J., Schnyder, J., Sobień, K., Koptíková, L., Krzemiński, L., Pszczółkowski, A., et al. (2013). Magnetic susceptibility and spectra gamma logs in the Tithonian–Berriasian pelagic carbonates in the Tatra Mts (Western Carpathians, Poland): Palaeoenvironmental changes at the Jurassic/Cretaceous boundary. *Cretaceous Research*, *43*, 1–17. https://doi.org/10.1016/j.cretres.2013.02.008

Grabowski, J., Stoykova, K., Wierzbowski, H., & Wójcik-Tabol, P. (2021). Upper Berriasian chemostratigraphy, clay minerals and calcareous nannofossils of the Barlya section (Western Balkan, Bulgaria): Implications for palaeoclimate and productivity changes, and stratigraphic correlations across the Alpine Tethys. *Palaeogeography, Palaeoclimatology, Palaeoecology*, *567*, 110252. https://doi.org/10.1016/j.palaeo.2021.110252

Gradstein, F. M., Ogg, J. G., Schmitz, M. D., & Ogg, G. M. (2020). *Geologic time scale 2020* (p. 1390). Elsevier. https://doi.org/10.1016/C2020-1-02369-3

Hallam, A. (2001). A review of the broad pattern of Jurassic sea-level changes and their possible causes in the light of current knowledge. *Palaeogeography, Palaeoclimatology, Palaeoecology*, *167*(1–2), 23–37. https://doi.org/10.1016/S0031-0182(00)00229-7

Hallam, A., Grose, J. A., & Ruffell, A. H. (1991). Palaeoclimatic significance of changes in clay mineralogy across the Jurassic-Cretaceous boundary in England and France. *Palaeogeography, Palaeoclimatology, Palaeoecology*, *81*(3–4), 173–187. https://doi.org/10.1016/0031-0182(91)90146-I

Haq, B. U. (2014). Cretaceous eustasy revisited. *Global and Planetary Change*, *113*, 44–58. https://doi.org/10.1016/j.gloplacha.2013.12.007

Haq, B. U. (2018). Jurassic Sea-Level Variations: A Reappraisal. *Geological Society of America Today*, *28*, 4–10. https://doi.org/10.1130/GSATG359A.1

Hardenbol, J., Thierry, J., Farley, M. B., de Graciansky, P.-C., & Vail, P. R. (1998). *Mesozoic and Cenozoic sequence chronostratigraphic framework of European basins* (Vol. 60, pp. 1–13). SEPM Special Publication. https://doi.org/10.2110/pec.98.02.0003

Hovikoski, J., Olivarius, M., Bojesen-Koefoed, J. A., Piasecki, S., Alsen, P., Fyhn, M. B. W., et al. (2023). Late Jurassic—Early Cretaceous marine deoxygenation in Northeast Greenland. *Journal of the Geological Society, London*, *180*(3). https://doi.org/10.1144/jgs2022-058

JASP Team. (2024). JASP (Version 0.19) [Computer software]. Retrieved from https://jasp-stats.org/

Jenkyns, H. C. (2010). Geochemistry of oceanic anoxic events. *Geochemistry, Geophysics, Geosystems*, *11*(3), Q03004. https://doi.org/10.1029/2009GC002788

Jones, B., & Manning, A. C. (1994). Comparison of geochemical indices used for the interpretation of palaeoredox conditions in ancient mudstones. *Chemical Geology*, *111*(1–4), 111–129. https://doi.org/10.1016/0009-2541(94)90085-X

Krische, O., Grabowski, J., Bujtor, L., & Gawlick, H.-J. (2018). Latest Jurassic to Early Cretaceous evolution in the central Northern Calcareous Alps. *Berichte der Geologischen Bundesanstalt*, *126*, 223–258.

Kumpan, T., Bábek, O., Kalvoda, J., Grygar, T. M., & Frýda, J. (2014). Sea-level and environmental changes around the Devonian–Carboniferous boundary in the Namur–Dinant Basin (S Belgium, NE France): A multi-proxy stratigraphic analysis of carbonate ramp archives and its use in regional and interregional correlations. *Sedimentary Geology*, *311*, 43–59. https://doi.org/10.1016/j.sedgeo.2014.06.007

Li, Y.-H., & Schoonmaker, J. E. (2003). Chemical compositions and mineralogy of marine sediments. *Treatise on Geochemistry*, *7*, 1–35. https://doi.org/10.1016/B0-08-043751-6/07088-2

Lodowski, D. G., & Grabowski, J. (2023). Tracing the latest Jurassic–earliest Cretaceous paleoenvironment evolution in carbonates: A case study of the Giewont succession (Central Western Carpathians, Poland). *Acta Geologica Polonica*, *73*, 741–772. https://doi.org/10.24425/agp.2023.145629

Lodowski, D. G., Grabowski, J., Rožič, B., Žvab-Rožič, P., Reháková, D., Slapnik, L., et al. (2024). Supporting Information: Sedimentary events at the Jurassic–Cretaceous transition in the Slovenian Basin (Alpine Atlantic): Further evidences for palaeoenvironmental record in pelagic sediments. *Zenodo*. https://doi.org/10.5281/zenodo.12542820

Lodowski, D. G., Pszczółkowski, A., Szives, O., Főzy, I., & Grabowski, J. (2022). Jurassic–Cretaceous transition in the Transdanubian Range (Hungary): Integrated stratigraphy and paleomagnetic study of the Hárskút and Lókút sections. *Newsletters on Stratigraphy*, *55*(1), 99–135. https://doi.org/10.1127/nos/2021/0656

Lodowski, D. G., Szives, O., Virág, A., & Grabowski, J. (2024). The latest Jurassic–earliest Cretaceous climate and oceanographic changes in the Western Tethys: The Transdanubian Range (Hungary) perspective. *Sedimentology*, *71*(6), 1843–1872. https://doi.org/10.1111/sed.13194

Meyer, K. M., & Kump, L. R. (2008). Oceanic Euxinia in Earth History: Causes and consequences. *Annual Review of Earth and Planetary Sciences*, *36*(1), 251–288. https://doi.org/10.1146/annurev.earth.36.031207.124256

Morales, C., Gardin, S., Schnyder, J., Spangenberg, J., Arnaud-Vanneau, A., Arnaud, H., et al. (2013). Berriasian and early Valanginian environmental change along a transect from the Jura Platform to the Vocontian Basin. *Sedimentology*, *60*(1), 36–63. https://doi.org/10.1111/sed.12019

Placer, L. (2008). Principles of the tectonic subdivision of Slovenia. *Geologija*, *51*(2), 205–217. https://doi.org/10.5474/geologija.2008.021

Price, G. D. (1999). The evidence and implications of polar ice during the Mesozoic. *Earth-Science Reviews*, *48*(3), 183–210. https://doi.org/10.1016/S0012-8252(99)00048-3

Price, G. D., Főzy, I., & Pálfy, J. (2016). Carbon cycle history through the Jurassic–Cretaceous boundary: A new global $\delta^{13}C$ stack. *Palaeogeography, Palaeoclimatology, Palaeoecology*, *451*, 46–61. https://doi.org/10.1016/j.palaeo.2016.03.016

Ray, D. C., van Buchem, F. S. P., Baines, G., Davies, A., Gréselle, B., Simmons, M. D., & Robson, C. (2019). The magnitude and cause of short-term eustatic Cretaceous sea-level change: A synthesis. *Earth-Science Reviews*, *197*, 102901. https://doi.org/10.1016/j.earscirev.2019.102901

Reháková, D., & Michalík, J. (1997). Evolution and distribution of calpionellids—The most characteristic constituents of Lower Cretaceous Tethyan microplankton. *Cretaceous Research*, *18*(3), 493–504. https://doi.org/10.1006/cres.1997.0067

Reháková, D., & Rožič, B. (2019). Calpionellid biostratigraphy and sedimentation of the Biancone limestone from the Rudnica Anticline (Sava Folds, eastern Slovenia). *Geologija*, *62*(1), 89–101. https://doi.org/10.5474/geologija.2019.004

Riboulleau, A., Baudin, F., Deconinck, J.-F., Derenne, S., Largeau, C., & Tribovillard, N. (2003). Depositional conditions and organic matter preservation pathways in an epicontinental environment: The Upper Jurassic Kashpir Oil Shales (Volga Basin, Russia). *Palaeogeography, Palaeoclimatology, Palaeoecology*, *197*(3–4), 171–197. https://doi.org/10.1016/S0031-0182(03)00460-7

Rider, M. (1990). Gamma-ray log shape used as a facies indicator: Critical analysis of an oversimplified method. *Geological Society, London, Special Publications*, *48*(1), 27–37. https://doi.org/10.1144/GSL.SP.1990.048.01.0

Rogov, M., Ershova, V., Vereshchagin, O., Vasileva, K., Mikhailova, K., & Krylov, A. (2021). Database of global glendonite and ikaite records throughout the Phanerozoic. *Earth System Science Data*, *13*(2), 343–356. https://doi.org/10.5194/essd-13-343-2021

Rogov, M. A., Ershova, V. B., Shchepetova, E. V., Zakharov, V. A., Pokrovsky, B. G., & Khudoley, A. K. (2017). Earliest Cretaceous (late Berriasian) glendonites from Northeast Siberia revise the timing of initiation of transient Early Cretaceous cooling in the high latitudes. *Cretacaceous Research*, *71*, 102–112. https://doi.org/10.1016/j.cretres.2016.11.011

Rožič, B. (2005). Albian–Cenomanian resedimented limestone in the Lower flyshoid Formation of the Mt. Mrzli Vrh Area (Tolmin region, NW Slovenia). *Geologija*, *48*(2), 193–210. https://doi.org/10.5474/geologija.2005.017

Rožič, B. (2009). Perbla and Tolmin formations: Revised Toarcian to Tithonian stratigraphy of the Tolmin Basin (NW Slovenia) and regional correlations. *Bulletin de la Societe Geologique de France*, *180*(5), 411–430. https://doi.org/10.2113/gssgfbull.180.5.411

Rožič, B. (2016). Paleogeographic units. In M. Novak & N. Rman (Eds.), *Geological atlas of Slovenia* (pp. 14–15). Geološki zavod Slovenije.

Rožič, B., & Šmuc, A. (2011). Gravity-flow deposits in the Toarcian Perbla formation (Slovenian basin, NW Slovenia). *Rivisita Italiana di Paleontologia e Stratigrafia*, *117*(2), 283–294. https://doi.org/10.13130/2039-4942/5975

Ruffel, A., McKinley, J. M., & Worden, R. H. (2002). Comparison of clay mineral stratigraphy to other proxy palaeoclimate indicators in the Mesozoic of NW Europe. *Philosophical Transactions of the Royal Society of London - A*, *360*, 675–693. https://doi.org/10.1098/rsta.2001.0961

Ruffel, A., & Worden, R. (2000). Palaeoclimate analysis using spectral gamma-ray data from the Aptian (Cretaceous) of southern England and southern France. *Palaeogeography, Palaeoclimatology, Palaeoecology*, *155*(3–4), 265–283. https://doi.org/10.1016/S0031-0182(99)00119-4

Schneider, A. C., Heimhofer, U., Heunisch, C., & Mutterlose, J. (2018). From arid to humid—The Jurassic-Cretaceous boundary interval in northern Germany. *Review of Palaeobotany and Palynology*, *255*, 57–69. https://doi.org/10.1016/j.revpalbo.2018.04.008

Schnetger, B., Brumsack, H.-J., Schale, H., Hinrichs, J., & Dittert, L. (2000). Geochemical characteristics of deep-sea sediments from the Arabian Sea: A high-resolution study. *Deep-Sea Research II*, *47*(14), 2735–2768. https://doi.org/10.1016/S0967-0645(00)00047-3

Schnyder, J., Ruffel, A., Deconinck, J.-F., & Baudin, F. (2006). Conjuctive use of spectral gamma-ray logs and clay mineralogy in defining late Jurassic–early Cretaceous paleoclimate change (Dorset, U.K.). *Palaeogeography, Palaeoclimatology, Palaeoecology*, *229*(4), 303–320. https://doi.org/10.1016/j.palaeo.2005.06.027

Scotese, C. R., Song, H., Mills, B. J. W., & van der Meer, D. G. (2021). Phanerozoic paleotemperatures: The Earth's changing climate during the last 540 million years. *Earth-Science Reviews*, *215*, 103503. https://doi.org/10.1016/j.earscirev.2021.103503

Shen, J., Schoepfer, S. D., Feng, Q., Zhou, L., Yu, J., Song, H., et al. (2015). Marine productivity changes during the end-Permian crisis and Early Triassic recovery. *Earth-Science Reviews*, *149*, 136–162. https://doi.org/10.1016/j.earscirev.2014.11.002

Tribovillard, N., Algeo, T. J., Lyons, T., & Riboulleau, A. (2006). Trace metals as paleoredox and paleoproductivity proxies: An update. *Chemical Geology*, *232*(1–2), 12–32. https://doi.org/10.1016/j.chemgeo.2006.02.012

Trujillo, A. P., & Thurman, H. V. (2011). *Essentials of Oceanography*. Prentice Hall.

van der Meer, D. G., Scotese, C. R., Mills, B. J. W., Sluijs, A., van der Berg van Saparoea, A.-P., & van de Weg, R. M. B. (2022). Long-term Phanerozoic global mean sea-level: Insights from strontium isotope variations and estimates of continental glaciation. *Gondwana Research*, *111*, 103–121. https://doi.org/10.1016/j.gr.2022.07.014

Vrabec, M., Šmuc, A., Pleničar, M., & Buser, S. (2009). Geological evolution of Slovenia—An overview. In M. Pleničar, O. Nojan, M. Novak, & S. Pirc (Eds.), *The Geology of Slovenia*. Geološki zavod Slovenije. Chapter 1.

Wei, G., Li, X.-H., Liu, Y., Shao, L., & Liang, X. (2006). Geochemical record of chemical weathering and monsoon climate change since the early Miocene in the South China. *Paleoceanography*, *21*(4), PA4214. https://doi.org/10.1029/2006PA001300

Weissert, H., & Erba, E. (2004). Volcanism, CO_2 and palaeoclimate: A Late Jurassic–Early Cretaceous carbon and oxygen isotope record. *Journal of the Geological Society, London*, *161*(4), 695–702. https://doi.org/10.1144/0016-764903-087

Weissert, H., & Mohr, H. (1996). Late Jurassic climate and its impact on carbon cycling. *Palaeogeography, Palaeoclimatology, Palaeoecology*, *122*(1–4), 27–43. https://doi.org/10.1016/0031-0182(95)00088-7

Wimbledon, W. A. P., Elbra, T., Pruner, P., Schnabl, P., Kdýr, Š., Šifnerová, K., et al. (2024). A re-description of the historical stratotype for the Berriasian Stage (Cretaceous System): Biostratigraphy and magnetostratigraphy. *Cretaceous Research*, *160*, 105892. https://doi.org/10.1016/j.cretres.2024.105892

Wimbledon, W. A. P., Reháková, D., Svobodová, A., Elbra, T., Schnabl, P., Pruner, P., et al. (2020). The Proposal of a GSSP for the Berriasian Stage (Cretaceous System): Part 1. *Volumina Jurassica*, *XVIII*(2), 53–106. https://doi.org/10.7306/VJ.18.7